REPORT DOCUMENTATION PAGE

Form Approved OMB NO. 0704-0188

1. REPORT DATE (DD-MM-YYYY)	2. REPORT TYPE	3. DATES COVERED (From - To)
21-12-2019	Final Report	1-Sep-2015 - 31-Aug-2019

4. TITLE AND SUBTITLE
Final Report: Spatially and Temporally Resolved Imaging of Primary Breakup in High-Pressure Fuel Sprays

5a. CONTRACT NUMBER
W911NF-15-1-0500

5b. GRANT NUMBER

5c. PROGRAM ELEMENT NUMBER
611102

6. AUTHORS

5d. PROJECT NUMBER

5e. TASK NUMBER

5f. WORK UNIT NUMBER

7. PERFORMING ORGANIZATION NAMES AND ADDRESSES
Georgia Tech Research Corporation
505 Tenth Street NW

Atlanta, GA 30332 -0420

8. PERFORMING ORGANIZATION REPORT NUMBER

9. SPONSORING/MONITORING AGENCY NAME(S) AND ADDRESS (ES)
U.S. Army Research Office
P.O. Box 12211
Research Triangle Park, NC 27709-2211

10. SPONSOR/MONITOR'S ACRONYM(S)
ARO

11. SPONSOR/MONITOR'S REPORT NUMBER(S)
66736-EG-YIP.2

12. DISTRIBUTION AVAILIBILITY STATEMENT
Approved for public release; distribution is unlimited.

13. SUPPLEMENTARY NOTES
The views, opinions and/or findings contained in this report are those of the author(s) and should not contrued as an official Department of the Army position, policy or decision, unless so designated by other documentation.

14. ABSTRACT

15. SUBJECT TERMS

16. SECURITY CLASSIFICATION OF:			17. LIMITATION OF ABSTRACT	15. NUMBER OF PAGES	19a. NAME OF RESPONSIBLE PERSON
a. REPORT	b. ABSTRACT	c. THIS PAGE			Caroline Genzale
UU	UU	UU	UU		19b. TELEPHONE NUMBER 404-894-5099

RPPR Final Report
as of 06-Jan-2020

Agency Code:

Proposal Number: 66736EGYIP **Agreement Number: W911NF-15-1-0500**
INVESTIGATOR(S):

Name: Caroline Genzale
Email: caroline.genzale@me.gatech.edu
Phone Number: 4048945099
Principal: Y

Organization: **Georgia Tech Research Corporation**
Address: 505 Tenth Street NW, Atlanta, GA 303320420
Country: USA

DUNS Number: 097394084 EIN: 580603146
Report Date: 30-Nov-2019 Date Received: 21-Dec-2019
Final Report for Period Beginning 01-Sep-2015 and Ending 31-Aug-2019
Title: Spatially and Temporally Resolved Imaging of Primary Breakup in High-Pressure Fuel Sprays
Begin Performance Period: 01-Sep-2015 **End Performance Period:** 31-Aug-2019
Report Term: 0-Other

Submitted By: Caroline Genzale Email: caroline.genzale@me.gatech.edu
Phone: (404) 894-5099

Distribution Statement: 1-Approved for public release; distribution is unlimited.

STEM Degrees: 3 **STEM Participants:** 4

Major Goals: Our primary objective is to demonstrate a new imaging diagnostic that can resolve primary atomization in a real-size diesel spray at O[um] spatial and O[ns] temporal resolution. To meet this objective, the major goals of this project are to: 1) develop a novel imaging system design to meet these measurement goals, 2) demonstrate the system to meet the proposed resolution objectives, 3) apply the developed tool to image real diesel sprays at engine-relevant conditions, and 3) compare our observations qualitatively and quantitatively against existing theoretical and experimental results.

Accomplishments: See .pdf document uploaded.

Training Opportunities: Two M.S. and two undergraduate students were trained under this project.

Results Dissemination: M.S. Theses:
Kim, Y. (2017). Development of Spectral Microscopy Imaging Technique for Time-Resolved Imaging of Primary Breakup in High-Pressure Fuel Sprays. M.S. Thesis. Georgia Institute of Technology, Atlanta, GA.

Maassen, K. (2020). High-Speed and High-Resolution Imaging of Primary Atomization in a Real Diesel Spray using Spectral Microscopy. M.S. Thesis. Georgia Institute of Technology, Atlanta, GA. (Expected publication in January 2020)

Refereed Conference Papers:
Maassen, K., Poursadegh, F. and Genzale, C.L., “Spectral Microscopy Imaging System for High-Resolution High-Speed Imaging of Fuel Sprays, “ ASME Internal Combustion Engine Division Fall Technical Conference, Chicago, IL, October 20-23, 2019.

Posters:
Maassen, K., Poursadegh, F., and Genzale C.L., “Spectral Microscopy for High Resolution, High-Speed Imaging of Primary Breakup in Fuel Sprays,” ILASS Americas 2019, Tempe, AZ, May 2019.

Honors and Awards: Nothing to Report

Protocol Activity Status:

RPPR Final Report
as of 06-Jan-2020

Technology Transfer: Nothing to Report

PARTICIPANTS:

Participant Type: Graduate Student (research assistant)
Participant: Yoontak Kim
Person Months Worked: 15.00 **Funding Support:**
Project Contribution:
International Collaboration:
International Travel:
National Academy Member: N
Other Collaborators:

Participant Type: Graduate Student (research assistant)
Participant: Kenneth Maassen
Person Months Worked: 15.00 **Funding Support:**
Project Contribution:
International Collaboration:
International Travel:
National Academy Member: N
Other Collaborators:

Participant Type: Undergraduate Student
Participant: Samuel Gilmer
Person Months Worked: 2.00 **Funding Support:**
Project Contribution:
International Collaboration:
International Travel:
National Academy Member: N
Other Collaborators:

Participant Type: Undergraduate Student
Participant: Henry Scott
Person Months Worked: 1.00 **Funding Support:**
Project Contribution:
International Collaboration:
International Travel:
National Academy Member: N
Other Collaborators:

DISSERTATIONS:

Publication Type: Thesis or Dissertation
Institution: Georgia Institute of Technology
Date Received: 20-Feb-2019 Completion Date: 10/30/17 11:59PM
Title: Development of Spectral Microscopy Imaging Technique for Time-Resolved Imaging of Primary Breakup in High-Pressure Fuel Sprays
Authors: Yoontak Kim
Acknowledged Federal Support: **N**

RPPR Final Report
as of 06-Jan-2020

Final Report - Grant # W911NF-15-1-0500
Project Period: Sept 1, 2015 – Aug 31, 2019

Spatially and Temporally-Resolved Imaging of Primary Breakup in High-Pressure Fuel Sprays

Caroline L. Genzale
Associate Professor
G.W. Woodruff School of Mechanical Engineering
Georgia Institute of Technology, Atlanta, GA, 30332

Summary

The primary objective is this work is to enable the measurement of primary breakup in real diesel sprays. This knowledge is needed to understand how non-traditional fuels, or even conventional fuels with physical property variations, affect fuel-air preparation and combustion in diesel engines. Such measurements are also needed to formulate more accurate atomization models for diesel-spray combustion simulations. These objectives support Army initiatives to streamline fuel supplies according the Single-Fuel Concept and enable use of non-traditional fuels. To meet these objectives, we develop a high-resolution imaging technique, termed Spectral Microscopy, that can quantify the complex and stochastic process of liquid jet disintegration in real-size diesel sprays at engine-relevant backpressures. The Spectral Microscopy imaging system couples wavelength-tuned ns-scale pulsed illumination with a custom microscopic lens and high-resolution 24 MP still-frame commercial-grade color camera. The system achieves an resolving power down to 1 μm, capturing three-image sequences at speeds of up to 13 Mfps. The newly-developed diagnostic is demonstrated by imaging primary atomization in real diesel sprays injected into engine-relevant high-pressure gas environments.

Table of Contents

Statement of the Problem Studied

Experiments to date have not resolved the primary breakup process of engine-relevant high-pressure liquid jets. Rather, our understanding of atomization in engine sprays has been established from either scaled-up low-velocity liquid jet experiments [1,2,3] or qualitative interpretation of macro-scale spray characteristics (e.g., spreading angle and spray penetration rate) [4,5,6]. Neither of these approaches has advanced our understanding of atomization well enough to achieve predictive spray models for internal combustion engine simulations [7,8,9], suggesting that physical theories developed from these data are incomplete and/or incorrect. To advance understanding, a diagnostic is needed with sufficient resolution for the study of primary atomization in real-size fuel sprays.

Since the breakup of an engine-relevant high-pressure liquid jet it expected to form a highly stochastic field of rapidly-evolving non-spherical micron-scale structures [1,2,10,11], it is critical to develop imaging diagnostics that are capable of high spatial and temporal resolutions. Towards this goal, our primary objective is to demonstrate a new imaging diagnostic that can resolve primary atomization in a real-size diesel spray at *O*[μm] spatial and *O*[ns] temporal resolution. In this work we, 1) develop an approach to meet these measurement goals, 2) apply the developed tool to image real diesel sprays at engine-relevant conditions, and 3) compare our observations qualitatively and quantitatively against existing theoretical and experimental results.

1 Background

1.1 Resolution Requirements for Imaging Diesel Spray Primary Atomization

While a number of prior researchers have applied various imaging techniques to study real-size fuel sprays [12,13,14,15], none of these diagnostics has successfully resolved the spatial and temporal evolution of primary atomization in these sprays. In this section, we estimate the resolution performance necessary to accomplish this, and set clear goals for the diagnostic-development pathway.

First, we estimate the spatial and temporal resolution needed to resolve the shape and size of liquid primary atomization structures (e.g., ligaments and droplets) and freeze their motion within the exposure time to avoid motion blur. Although the process of primary atomization has not been well imaged, isolated ligaments and droplets resulting from the process have been resolved and there is consensus in experimental results that ligament and droplet diameters in these sprays are on the order of μm [16,17]. For sake of estimating flow time scales, the Bernoulli equation is used to estimate the injector exit-flow velocity. For the fuel used in this work, n-dodecane, the Bernoulli velocity with respect to fuel pressure (injecting into air at STP) is shown in **Figure 1**. Note that the units in **Figure 1** are μm/ns.

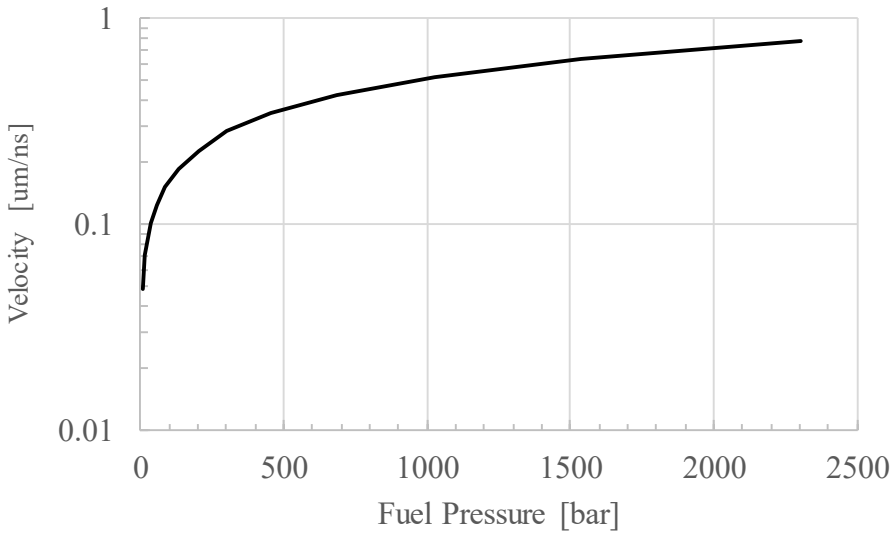

Figure 1: Bernoulli velocity of an n-dodecane spray as a function of fuel pressure, assuming it is injected into ambient air at STP.

The most challenging features to image are the fastest and smallest droplets, theoretically ~1 μm in diameter and traveling at speeds of ~600 m/s. To prevent motion blur, object motion should be restricted to less than one pixel length over the course of the exposure duration. The acceptable exposure time is therefore dependent on magnification, but for a general target of pixel resolution < 1 μm/px, exposure duration should be on the ns timescale. For frame-to-frame tracking, it is important to capture movement on the scale of an object's size. For objects with diameters between 1 and 10 microns, with velocities between 0.1 and 1 μm/ns, inter-frame timing will need to be on the order of 10-100 ns. This is equivalent to frame rates of 10-100 Million fps (Mfps).

Another technical challenge in imaging primary atomization is digital image resolution. Digital image resolution sets a limit on the field-of-view (FOV), or the magnification of the system in [μm/px]. For example, on a 1 MP image sensor that is 1000 pixels wide, a magnification of 0.5 μm/px would have a FOV of 500 microns. This significantly limits the ability to track flow information, as features will quickly travel out of this FOV. If the magnification is further increased to 0.2 μm/pix to give better resolution of droplet diameters and shape, the FOV would be 200 μm and we would be unable to see the full height of a spray. To study primary atomization with μm scale ligaments moving at μm/ns velocities, image resolutions on the order of 10 Megapixels are needed to best track flow information. Based on these estimates, a summary of the performance goals for the Spectral Microscopy system are given in **Table** 1.

Table 1: Diagnostic performance goals to study primary atomization in real-size fuel sprays

Metric	Goal
Image Size	> 2000 x 2000 px
Frame Rate	> 10 Mfps
Resolution	< 2 μm
Exposure Time	< 10 ns

1.2 Quantifying Resolution of an Imaging System

The fundamental limit of resolving power for an imaging system is determined by the behavior of light as it passes through an aperture. As an image passes through an aperture, it is distorted via diffraction. Because of diffraction at the aperture, the image of a point source captured by a camera is comprised of sequence of concentric airy disks, with the diameter of these disks a function of the aperture geometry and light wavelength. The minimum airy disk diameter is known as the Abbe diffraction limit, given in Eq. (1). For visible-light microscopy, the wavelength of light is limited to 400 and 700 μm, and the Numerical Aperture (NA) of the system limits the optical resolving power.

$$L_{Abbe}[\mu m] = \frac{\lambda\,[\mu m]}{2\,NA\,[-]} \tag{1}$$

The other limit of a system's resolving power is the Nyquist limit, defined as twice the sampling frequency, f_{img}, given in (μm/px) in Eq. (2). While the Nyquist limit is commonly used to define the maximum resolvable frequency in 1-D data sets, the discrete sampling nature of 2-D digital images also sets a limit on the maximum resolvable frequency in an image (or smallest resolvable feature). This limit can be changed by increasing the image magnification. However, this reduces the FOV and also reduces incident light per pixel, which can decrease image quality.

$$L_{nyq}[\mu m] = 2f_{img}\left[\frac{\mu m}{px}\right] \tag{2}$$

Ultimately, the resolving power of an imaging system should be experimentally quantified to assess the practical system-level response. Resolving power goes beyond image resolution (μm/px), and includes factors like the quality of lenses, optical or diffraction limits, and the light throughput of the system. While there are multiple methods for quantifying image resolution, such as imaging a calibrated chart [18], the most versatile and accepted resolution quantification is the Modulation Transfer Function (MTF) [19]. In essence, the MTF quantifies edge resolution and contrast transfer through the optical system from the image of a sloped knife edge. The method to quantify the MTF is illustrated in **Figure 2.**

There are multiple steps in calculating the MTF. First, an area subset of the sloped knife edge image is selected, as shown in **Figure 2(a)**. In this example, the edge of an etched line on a slanted USAF target is used. To obtain the edge spread function, shown in **Figure 2(b)**, the perpendicular distance from the edge to each pixel is calculated, and the intensity is plotted with respect to distance from the edge. The line spread function (LSF), shown in **Figure 2(c)**, is obtained by taking the derivative of the edge spread function and applying a centered hamming window, which isolates the signal at the edge. The peak in the LSF correlates with the maximum slope of the ESF (**Figure 2(b)**). Finally, the MTF, shown in **Figure 2(d)**, is calculated with a Fast Fourier Transform of the LSF [18], which then quantifies contrast transfer as a function of spatial frequency. Thus, an imaging system with higher spatial resolution and sharper edge detection will have higher MTF at higher spatial frequencies (given in line-pairs/mm). To report a single numerical value for the measured resolution, a 10 percent criteria is used [19], shown as a dashed line in **Figure 2(d)**. In the example shown, the MTF at 10% contrast transfer is approximately 600 line-pairs/mm (LPMM), which is equal to a spatial resolution of 0.83 μm. The MTF in this work is calculated using the pre-packaged esfrmat3 code from the ISO standard 12233, and the 10 percent criteria is interpolated in MATLAB [18].

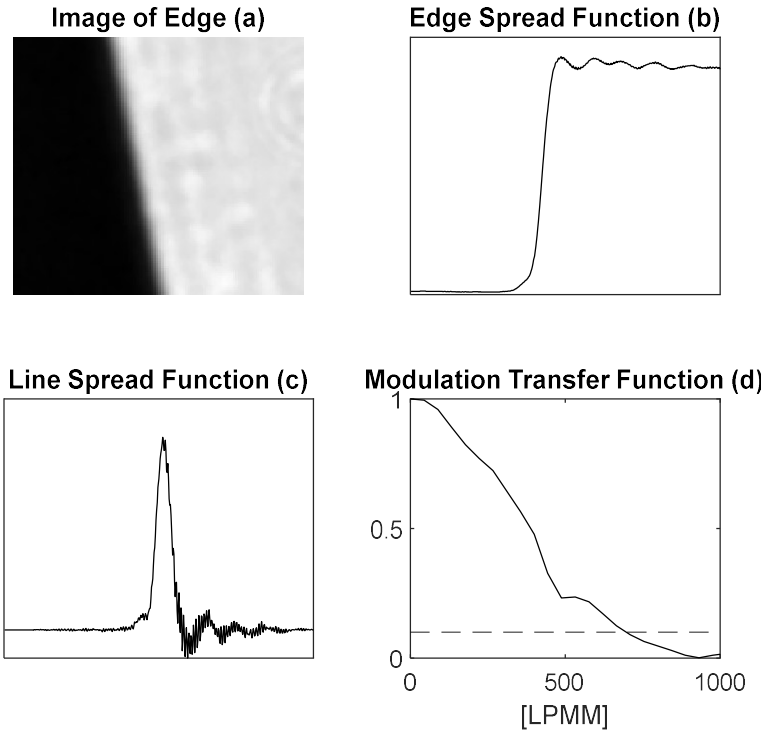

Figure 2: The four steps in computing the Modulation Transfer Function: The original image (a), Edge Spread Function (b), Line Spread Function (c), and the Modulation Transfer Function (d).

2 Approach

2.1 Spectral Microscopy Concept

Our overall approach to achieve the imaging resolutions and diagnostic targets in this work (**Table 1**) is shown schematically in **Figure 3**. The approach, termed Spectral Microscopy, utilizes ns-pulsed colored illumination that is wavelength-matched to the color detection channels of a consumer-grade high-resolution 24-MP color camera (Nikon D5300 DLSR). Using a color camera with an RGB Bayer Filter, a pulsed illumination sequence from three colored light sources (e.g., red, green, and blue wavelengths) generates three temporally-separated images that are encoded onto a single sensor by the Bayer Filter. Linear algebra is then used to extract the three images (RGB) and reconstruct the temporal sequence. This approach is inspired by other uses of image color-coding in the literature, where this type of concept has been used for PIV [20,21] and larger-scale flow imaging [22]. It is especially advantageous for high-speed microscopy because high-speed cameras often operate with limited sensor areas (typically < 1 MP). This makes it difficult to produce image resolutions that match the optical resolution capabilities of a quality high-magnification microscopy lens, making most microscopy setups Nyquist limited. Spectral microscopy decouples the job of temporal resolution from the camera, such that the temporal resolution of the diagnostic is solely determined by the pulse-duration and pulse-separation capabilities of the illumination system, while use of a high-resolution still-frame camera enables Abbe diffraction-limited spatial resolutions determined by the optics.

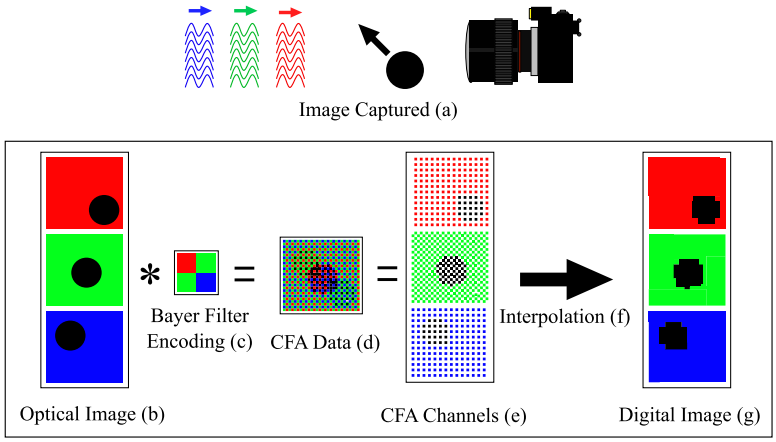

Figure 3: Spectral Microscopy encodes three temporally-separated frames in a single high-resolution image file. An optical image sequence is generated used pulsed colored light that is wavelength-tuned to match the detection channels of a color camera. In this example, pulsed illumination is selected in red, green, and blue wavelengths to match the RGB detection bands of a Bayer Filter. The optical image sequence (b) is encoded with the Bayer Filter (c) and stored in the Color Filter Array (CFA) (d). The CFA is then demosaiced to reconstruct the optical image sequence.

2.2 System Design Approach

The Spectral Microscopy concept relies on matching illumination wavelengths with the color detection bands of the camera's image sensor. Based on a cost-benefit assessment of available scientific and consumer-grade color cameras with a minimum sensor resolution of 10 MP (see diagnostic goals in **Table 1**), a consumer-grade 24-MP DLSR Nikon 5300 was specified for this project. Because Nikon does not provide sensor-specific quantum efficiency data, the detection sensitivity as a function of illumination wavelength (spectral sensitivity) was measured using a monochromator (Perkin-Elmer 650S) following [23]. Illumination from the monochromator was

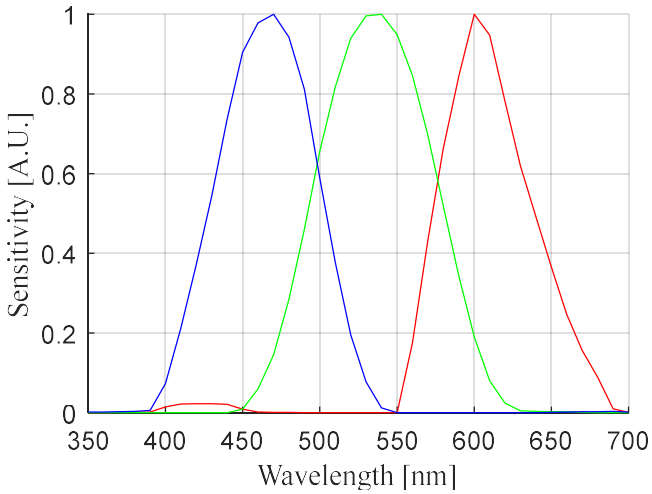

Figure 4: Measured spectral sensitivity [a.u] of Nikon D5300. Illumination wavelengths for Spectral Microscopy were selected to avoid color crosstalk, while balancing maximum transmission near the peak detection sensitivity. In Phase 1 of this project, LEDs with emission wavelengths of 627 nm, 530 nm, and 447.5 nm were used. In Phase 2, a laser-pulsed fluorescence illumination system was designed to emit light at 690 nm, 560 nm, and 420 nm.

passed into an integrated sphere and imaged from an orthogonal exit port using a microscopic lens and the Nikon D5300. The monochromater was swept over the visible range of wavelengths and multiple images were recorded at each illumination wavelength to assess shot-to-shot variation. The camera ISO was set to 100 to minimize the noise amplification and the shutter speed was set to 3 seconds to maximize the measured light intensity without producing saturation. Images were stored in the Nikon proprietary .NEF format and converted into a more universal .tiff format. The .tiff files where then demosaiced using MATLAB to separate the red, green, and blue image channels. A dark frame was subtracted from each image to remove thermal noise and the intensity of each image was then averaged over the field of view to quantify the average intensity recorded at a given illumination wavelength.

Figure 4 shows the measured spectral sensitivity of the Nikon D5300 CMOS sensor over the visible range of wavelengths. Because an optical power calibration was not performed, the units of measured intensity is given in arbitrary units [a.u.]. Peak sensitivities were recorded at 600 nm, 535 nm, and 470 nm for the red, green, and blue channels, respectively. There is also cross-talk evident between the blue-green channels and the green-red channels. Cross-talk is managed via post-processing, as discussed in Section 2.3.

Two different pulsed illumination systems were designed and assessed as part of this project. In our first design of the Spectral Microscopy system (Phase 1), we targeted the use of a cost-effective and simple-to-implement high-power pulsed LED illumination system, paired with a consumer-grade 24 MP DSLR color camera (Nikon D5300). **Figure 5** shows the overall diagnostic setup. The high-power pulsed LEDs (Lightspeed Technologies) were specified at wavelengths of 627 nm, 530 nm, and 447.5 nm, with manufacturer-specified emission bandwidths of approximately 10 nm. Dichroic mirrors are used to overlap red, green, and blue illumination along the same optical path through the spray, while a field condenser lens focuses the illumination at the object plane (spray) to optimize illumination across the field-of-view. The field condenser lens is matched to the numerical aperture of the microscopic lens to optimize light throughput of the system. The pulsed LED system is capable of commanding 10-ns light

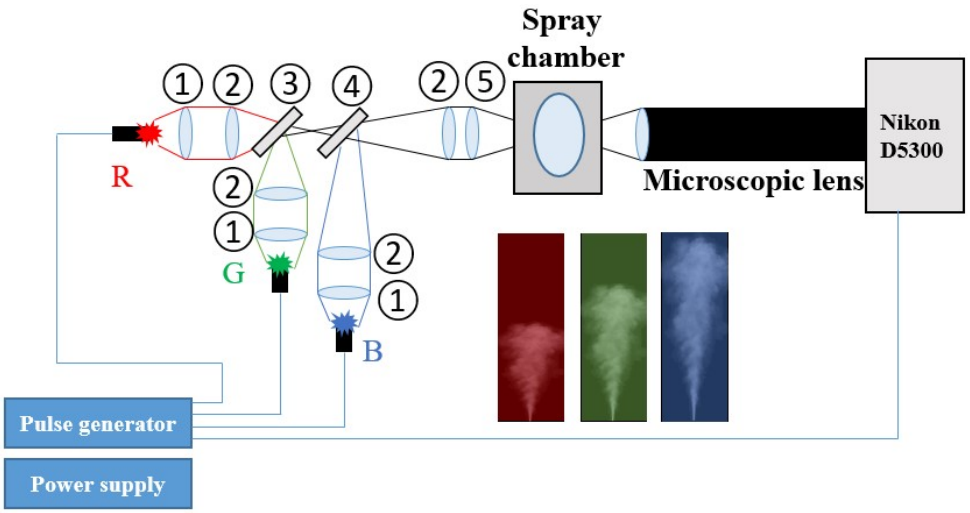

Figure 5: Optical setup for Spectral Microscopy using high-power pulsed LED illumination (Lightspeed Technologies), paired with a commercially-available microscopy lens (Infinity Photo-Optical Company). Overall experimental setup includes, ① condensing lens (f=32 mm, D=50 mm), ② focusing/collimating lenses (f=125 mm, D=50.8 mm), ③ long-pass dichroic mirror (605 nm), ④ long-pass dichroic mirror (505 nm), ⑤ field condenser lens (f=317.5 mm, effective diameter = 50.8 mm).

pulses via a pulse generator. The working distance of the commercially-available microscopic lens (Infinity K2 Distamax) was 228 mm, with a numerical aperture (NA) of 0.083 and 1.4x magnification. The long working distance of the lens enabled use with the high-pressure spray chamber in our lab (radius of 222 mm to outside surface of optical window) to enable imaging at engine-relevant high-pressure conditions. As we discuss further in Section 4.1, the LED illumination system did not produce sufficient light throughput and this ultimately impacted the maximum achievable image contrast and resolution of this system design.

To address the need for increased light throughput, we modified the illumination scheme in our second design of the Spectral Microscopy system (Phase 2) to use three Q-switched pulsed Nd:YAG lasers. The laser-illumination system was advanced in two sub-phases (Phase 2a and Phase 2b). The initial optical setup for laser illumination (Phase 2a design) is shown in **Figure 6**. Laser illumination applied in a backlit imaging arrangement, as used in this diagnostic setup, typically results in image speckle due to beam coherence, so the Nd:YAG ouput is passed through laser-fluorescing dye cells to both shift the emitted illumination wavelength and mitigate beam coherence. Three dyes were selected to emit Laser-Induced Fluorescence (LIF) (as excited by 355 nm or 532 nm output from an Nd:YAG) at wavelengths that matched the D5300 image sensor sensitivity (**Figure 4**). To produce red illumination, LD 690 Perchlorate dye (Exciton Luxottica) was excited by Nd:YAG illumination at 532 nm, producing a peak fluorescence output near 660 nm. To produce green illumination, Rhodamine 560 Chloride (Exciton Luxottica) was excited by Nd:YAG illumination at 532 nm, producing a peak fluorescence output near 560 nm. To produce blue illumination, Stillbene 420 dye (Exciton Luxottica) was excited by Nd:YAG illumination at 355 nm, producing a peak fluorescence output near 425 nm. The power output of each Nd:YAG was tuned to produce approximately equivalent detection intensity by each color channel (RGB) on the Nikon D5300 sensor.

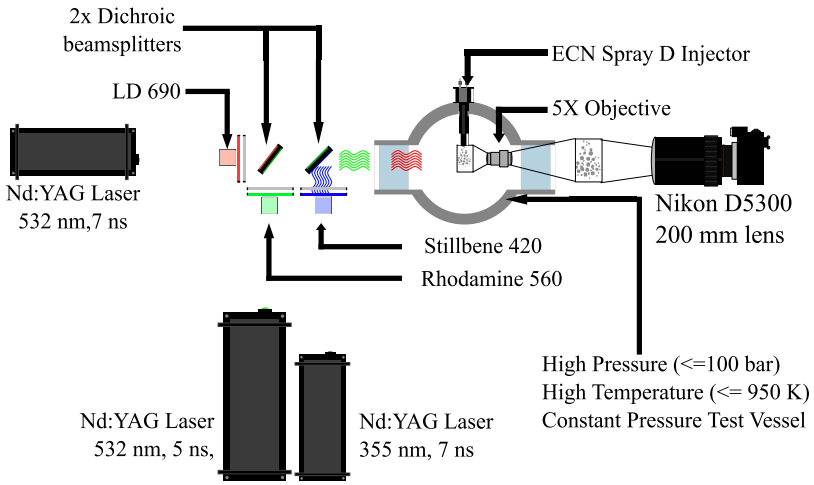

Figure 6: Phase 2a design of Spectral Microscopy system utilizing pulsed LIF illumination.

In the initial design (Phase 2a), the imaging system used unfocused LIF illumination and a custom two-piece microscopy lens (discussed further in Section 4.2), composed of a 5X microscope objective and a 200-mm focal-length lens (Nikkor). Images from this setup exhibited a few issues: loss of light through the system, lower resolving power, and some speckle effect from direct laser emission passing through the dye cells to the camera. These issues were addressed in a modified version of this illumination scheme in the Phase 2b design.

The Phase 2b design, shown in **Figure 7**, incorporated focusing lenses at the output of the LIF dye cells to improve light collection, and a field focusing lens to increase irradiance at the object plane and increase system light throughput. To address image speckle, the Nd:YAG pump beams where modified to strike the dyes cells at an oblique angle so that light from the laser was not directly transmitted to the camera. In this system design, the focused LIF illumination was passed through a second two-piece custom microscopy lens, composed of a 10x microscope objective and a 700-mm focal-length lens (Nikkor).

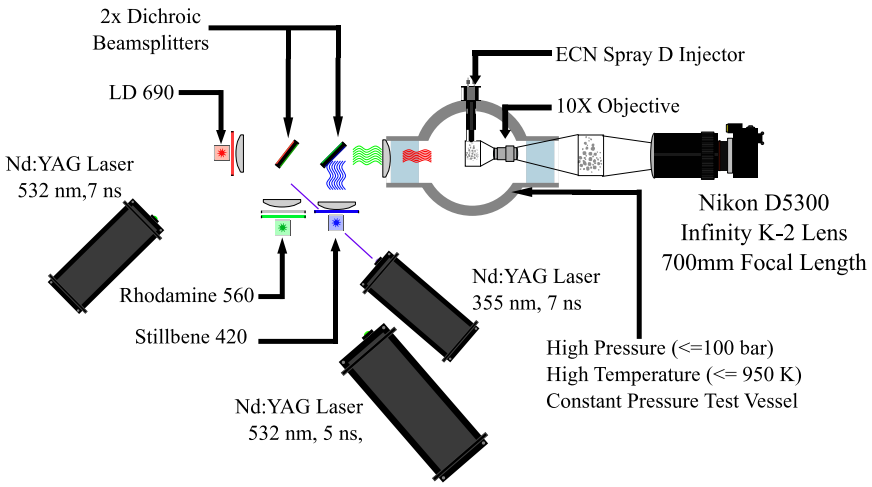

Figure 7: Phase 2b design of Spectral Microscopy imaging system. The lenses in the light train capture the emitted light from the dye cell and focus the light to the object plane. The oblique positioning of the lasers spatially filters the laser beam from the dye cell light.

2.3 Correcting for Color Cross Talk

Due to overlap in the spectral sensitivity curves for the RGB color channels of the Nikon D5300 image sensor (**Figure 4**), the demosaiced RGB channel images exhibit color cross-talk. Cross-talk was removed from each image via post-processing. To accomplish this, a calibration procedure was developed to quantify cross-talk intensities. Images were taken with a single backlight wavelength and the average red, green, and blue pixel response to each illumination wavelength was measured. The measured values for illumination with the Phase 1 LED system are shown in **Figure 8**, where the bars represent the normalized response of a pixel to the blue, green, and red LED backlights.

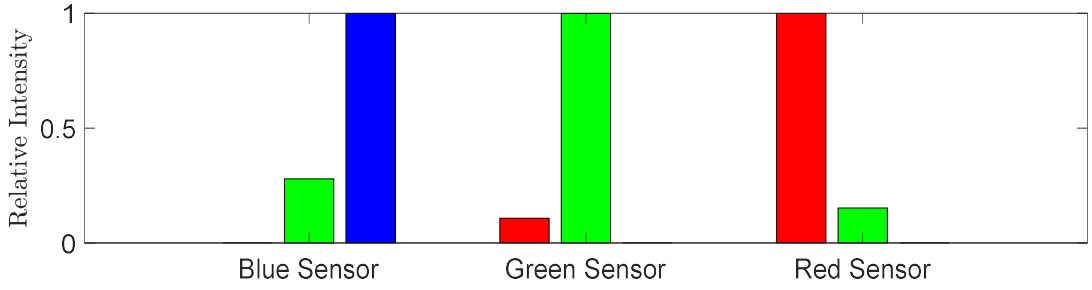

Figure 8: Average red, green, and blue pixel response of Nikon D5300 to the selected LED illumination wavelengths used in the Phase 1 design. In this setup, the green light source was detected in all three color channels.

Linear algebra is used to decouple the color cross-talk components of an image based on the known pixel response to the backlight colors [24,25]. The equation for converting the image recorded on each camera color channel (R_C, B_c, G_c,) to the optical image formed by each illumination wavelength (R_L, G_L, B_L,) is given in Eq. (3). In Eq. (3), X_{gr} represents the amount of green light captured on the red pixel relative to the amount of green light captured on the green pixel. For the case shown in Figure 8, [X_{gr}, X_{gg}, X_{gb}] = [0.2, 1, 0.35]. In Eq.(3), R_A is the stray light incident on the red pixel, including both dark-noise and room lighting. Since this system is running at low repetition rates (~ 0.25 Hz) in an ambient environment, the temperature dependence of dark noise is neglected.

$$\begin{bmatrix} R_c \\ G_c \\ B_c \end{bmatrix} = \begin{bmatrix} 1 & X_{rg} & X_{rb} \\ X_{gr} & 1 & X_{gb} \\ X_{br} & X_{bg} & 1 \end{bmatrix} \begin{bmatrix} R_L \\ G_L \\ B_L \end{bmatrix} + \begin{bmatrix} R_A \\ G_A \\ B_A \end{bmatrix} \quad (3)$$

3 Facility and Experimental Conditions

To study diesel spray primary atomization at engine-relevant conditions, fuel was injected into a high-pressure (> 10 bar) optically-accessible vessel at Georgia Tech. The vessel is also capable of generating high-temperature ambient conditions for combustion-relevant studies (> 900 K), but to avoid image defocusing and competing thermo-physical processes (e.g., vaporization), such conditions were not included in the current study. The capabilities of this vessel are further detailed in [26]. The fuel injector used in this study (ECN Spray D No. 133 [27]) has a 180-μm axially-drizzled single orifice and was supplied with n-dodecane fuel at pressures from 200 to 2000 bar. A general schematic of the experimental setup is shown in **Figure** 9.

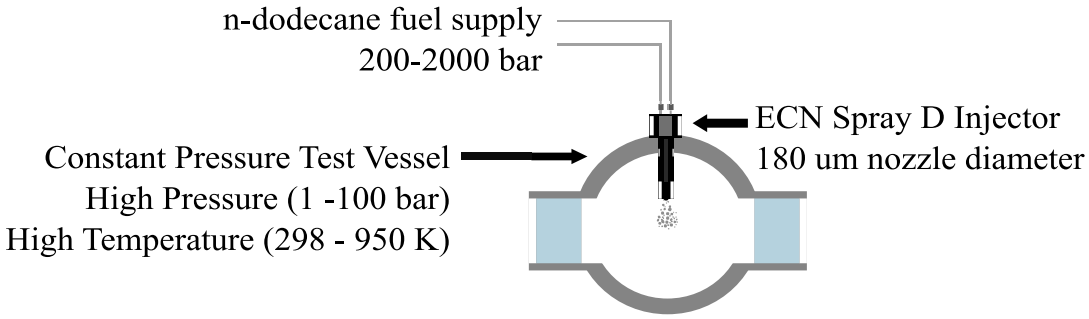

Figure 9: Experimental setup to study primary atomization at engine-relevant conditions.

In **Figure 10**, the operating conditions for all data sets taken for this project are shown as black circles on the regime diagram from Reitz [28]. All test conditions are in the atomization regime. As shown in **Figure 10**, because all experiments utilized dodecane fuel and a single-orifice injector (ECN Spray D, 180 μm orifice diameter), all conditions have a fixed Ohnesorge number of 0.021. The Reynolds numbers varied with fuel pressure (velocity, estimated via Bernoulli equation) and air pressure, and ranged from Re = 31,000 to 63,000. All data was obtained at standard temperature (298 K) but with varying backpressures. As shown in **Table 2**, spray imaging was conducted in two phases with two different optical system designs (Phase 2a and Phase 2b). During Phase 2a, spray imaging was conducted with a range of ambient backpressures. During Phase 2b, spray imaging was conducted under atmospheric backpressure conditions only.

Table 2: Operating conditions for Phase 2a and 2b spray imaging campaigns.

Project Phase	Fuel Pressure [bar]	Ambient Pressure [bar]	Inter-frame time [ns]
Phase 2a	500,1000,1500	2,6,20	300 (3 Mfps)
Phase 2b	350,500,1000,1500	1	75 (13 Mfps)

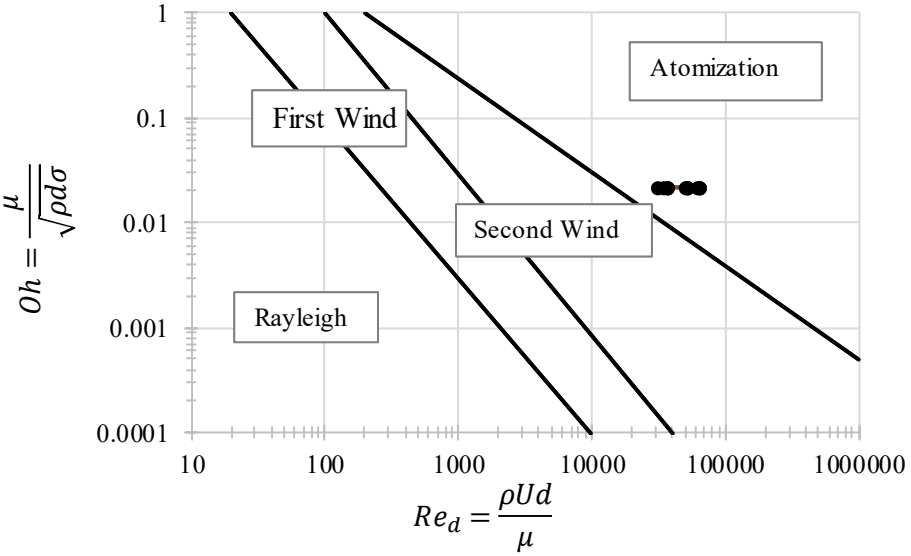

Figure 10: Test conditions for diesel spray primary atomization imaging (black circles). Regime diagram from Reitz [28].

4 Summary of Most Important Results

4.1 Spectral Microscopy Imaging with High-Power Pulsed-LED Illumination

In the first design phase of the Spectral Microscopy imaging system (Phase 1), we coupled a consumer-grade 24 MP DSLR color camera (Nikon D5300) with a commercially-available long-range microscopic lens (Infinity Distamax K2) and utilized a set of three high-power pulsed LEDs (Lightspeed Technologies) for RGB illumination with central emission wavelengths of 627 nm (red), 530 nm (green), and 447.5 nm (blue). The overall setup for this design was shown and discussed in **Figure 5.** Based on the NA of the microscope objective (NA = 0.083), the calculated Abbe diffraction-limited resolution of the system is 265 lpmm (Eq. (1)), or 1.9 μm, limited by the red LED illumination (shorter wavelengths increase the diffraction-limited resolution). The calculated Abbe resolution limit for all three light colors is shown at the top of **Table 3**. Unfortunately, the measured practical resolution of the system, quantified by the measured system resolution at 10% MTF (see Section 1.2), was substantially lower than this value.

Table 3: Calculated Abbe resolution and measured resolution of Phase 1 Spectral Microscopy system.

	Illumination Wavelength		
Resolution Criteria	Red (lpmm)	Green (lpmm)	Blue (lpmm)
Abbe Limit	265	314	370
10% MTF (at best focus for each color)	162	224	153
10% MTF (single image plane, pulsed illumination)	160	178	15
Nyquist Limit	350	495	350

To quantify the highest achievable resolution in practice with the Phase 1 Spectral Microscopy system, we measured the MTF response from the image of a slanted knife edge at the optimal focus position for each illumination wavelength. This measured result is shown in **Figure 11**, and the corresponding 10% MTF values are shown in the second row of **Table 3**. As shown, the Phase 1 design only achieved about half of the Abbe resolution. The primary reason for this was lack of transmitted image contrast due to low light throughput. The low NA of the microscopic lens demands high illumination power to achieve effective irradiance at the image sensor. During this design phase, we fully optimized the illumination optics train, including matching the NA of the field condenser lens to the microscope objective to minimize light loss and maximize light collection, but ultimately, the emitted power of the LEDs was insufficient to generate intensities greater than around 150 counts (~1% of the 14-bit sensor bandwidth) at a camera ISO setting of 100. An ISO value of 26500 (maximum for this sensor) was required to achieve intensities near 15,800 (97% of the sensor bandwidth). SNR was unacceptable at this ISO and significantly degraded the measured MTF.

We also discovered that the microscopic lens used in the Phase 1 design suffered from

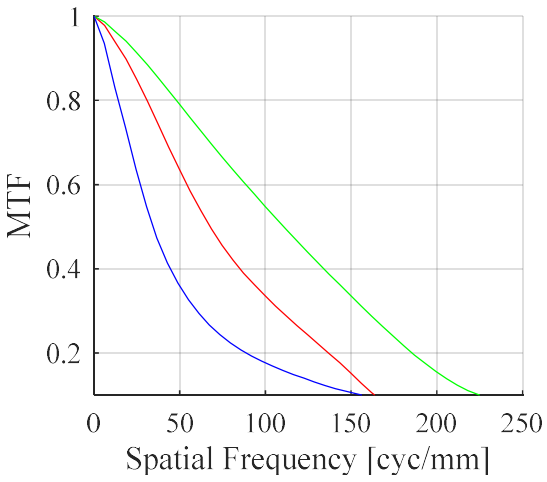

Figure 11: Measured MTF of Phase 1 Spectral Microscopy system at best focus position for each LED illumination wavelength.

severe longitudinal chromatic aberration. This issue is demonstrated in **Figure 12**, where the MTF was measured as a function of focus position for each illumination wavelength. In this plot, the 10% MTF resolution is quantified for each illumination wavelength over a range of focus positions (working distances). The measured 10% MTF values are then normalized to

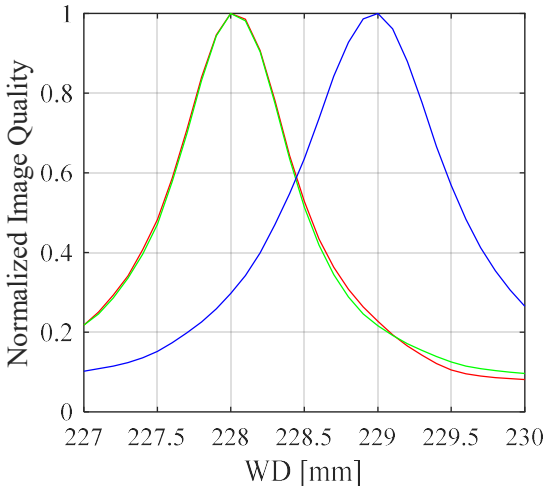

Figure 12: Measurement of longitudinal chromatic aberration using the Lightspeed K2 Distamax long-range micrcopic lens. The peak Normalized Image Quality indicates the best focus point (working distance) for each illumination wavelength (red, green, and blue LED light).

demonstrate the relative image quality (or Normalized Image Quality) as a function of working distance. The locations of peak Normalized Image Quality can then be interpreted as the optimal focus position. As shown, the optimal focus position for red and green illumination overlap, but the optimal focus position for blue illumination is shifted by approximately 1 mm. Furthermore, for a fixed focal position at the red/green best-focus position (as used in practice), the Normalized Image Quality with blue illumination is only 30% of that produced by red/green illumination.

This chromatic aberration effect is directly demonstrated in **Figure 13**, where the MTF was measured for each illumination wavelength used a fixed focal position. This measurement was further conducted with 10-ns pulsed light to evaluate the light throughput of pulsed

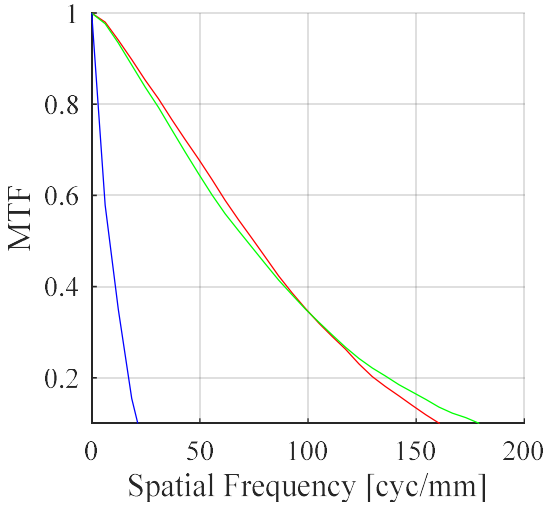

Figure 13: Measured MTF of Phase 1 Spectral Microscopy system at fixed focal position (WD=228 mm) using 10-ns pulsed LED illumination.

illumination (as used in practice with Spectral Microscopy) and it's effect on system resolution. As shown in **Figure 13**, the measured MTF curve with blue illumination is significantly degraded in this setup. The corresponding 10% MTF values for this setup are shown in the third row of **Table 3.** The blue-limited system resolution for the Phase 1 design was 15 lpmm (or 33 μm). This measured resolution is well below our diagnostic target of < 2 μm. Thus, this lens aberration, combined with the low power output of the pulsed LEDs, motivated a new design strategy for both the microscopic lens and the illumination system in Phase 2 of this project.

4.2 Novel Two-Piece Microscopy Lens Design

In the second design phase of the Spectral Microscopy imaging system (Phase 2), we designed a custom two-piece microscopic lens to address the chromatic aberration issues discovered during Phase 1. We also designed a pulsed-LIF illumination system (discussed in Section 2.2) to increase illumination power, with central emission wavelengths of approximately 660 nm (red), 560 nm (green), and 425 nm (blue). Two different variants of this overall design were shown and discussed in **Figure 6** and **Figure 7.**

The custom two-piece lens design was inspired by basic microscope design, where multi-piece lens designs are used to lower working distance and increases resolving power compared to a single lens [10]. Because an objective lens focuses an image of the object plane to infinity, image formation at the camera sensor is not sensitive to the relative distance between the objective and focusing/magnification lenses. As such, the objective can be physically separated from the main lens and mounted some distance away. In our case, as shown in **Figure 14**, this allows the objective to be mounted remotely from the main lens, placing it inside the chamber in close working distance to the spray. This enables the use of objectives with substantially higher magnification (and short working distances).The drawbacks of this design are increased difficulty in lens alignment and an increase in ambient light entering the main lens. This is overcome with careful alignment of the system and turning the lights off in the room, respectively.

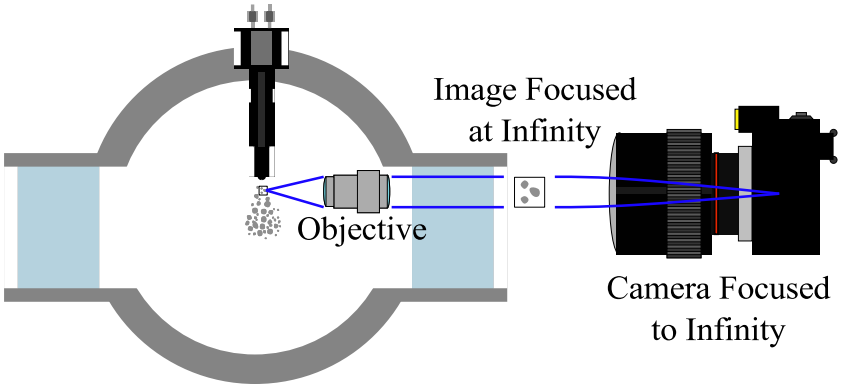

Figure 14: A multi-lens setup to maximize image resolution in a high-pressure spray experiment.

To specify the optimal combination of objective and camera lens to meet our diagnostic targets, we quantified the magnification and resolution limits of a two-piece lens system. The total magnification of the two-piece lens is a function of the objective magnification and the camera lens focal length. **Figure 15** demonstrates an experimental verification of total system magnification as a function of cameral focal length and objective magnification, determined by measuring bars on a USAF target and varying the main lens focal length with different objectives. Knowing the pixel pitch of the Nikon D5300 (3.89 μm), the Nyquist resolution limit

and the Abbe diffraction limit can be solved for as a function of lens configuration using Eq. (4) and Eq. (5), respectively.

$$L_{nyq} = \frac{2P_{px}x_1}{M_{obj}f} = \frac{2P_{px}f_{obj}}{f_1} \tag{4}$$

$$L_{Abbe} = \frac{\lambda}{2\,NA_{obj}} \tag{5}$$

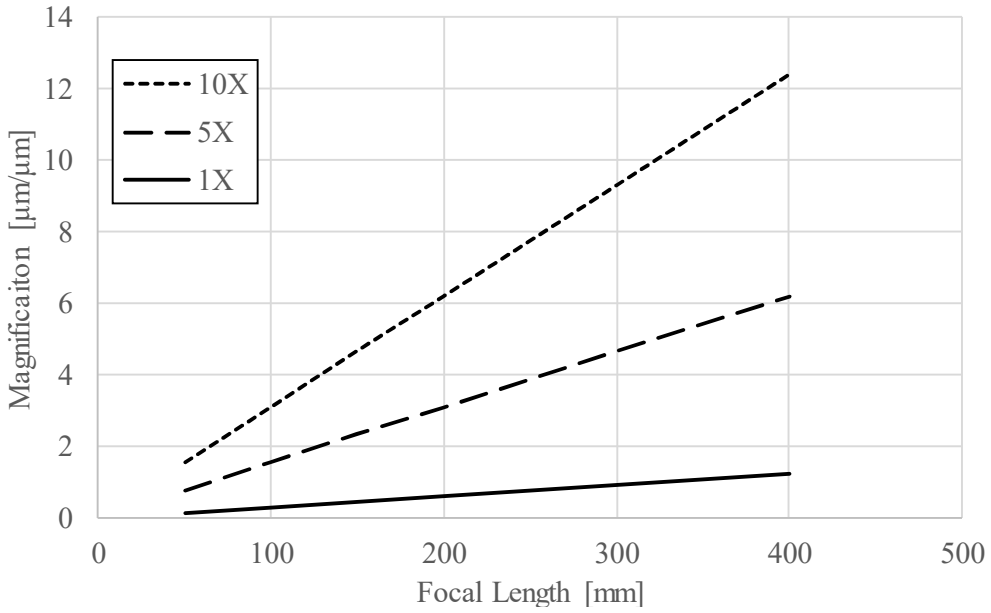

Figure 15: Total system magnification as a function of lens focal length and objective magnification.

Two multi-lens configurations were ultimately specified and used in this work. In the Phase 2a design, a 5X 0.21 NA objective lens was used with a f = 200 mm f/5.6 Nikkor camera lens (x_1=128 mm), yielding a 1.4 µm Abbe diffraction limit and a 2.8 µm Nyquist limit (2.8x magnification). In the Phase 2b design, we targeted the use of an objective with higher NA so that more light throughput and a higher diffraction limit could be reached. In Phase 2b, we employed a 700-mm camera lens (x_1= 350 mm) with a 10X 0.28 NA objective, resulting in a 1.2 µm Abbe limit and a 0.4 µm Nyquist limit (19.5x magnification).

To demonstrate system resolving power, images of a USAF target were taken with both the 5X+200-mm lens (Phase 2a) and the 10X+700-mm lens (Phase 2b). The USAF image taken with the 5X+200-mm lens and a 560-nm pulsed-LIF backlight is shown in **Figure 16**, and the image taken with the 10X+700-mm lens and a 450-nm pulsed-LIF backlight is shown in **Figure** 17. Note group 6 and 7 are barely visible in the right-most image of **Figure 16**, but are clearly readable in the central image of **Figure 17**. With the 10X+700-mm lens combination, the smallest resolvable bars are last two elements in group 8 (contained inside the red box shown in the central image of **Figure 17**), corresponding to line widths of 1.2 and 1.1 μm.

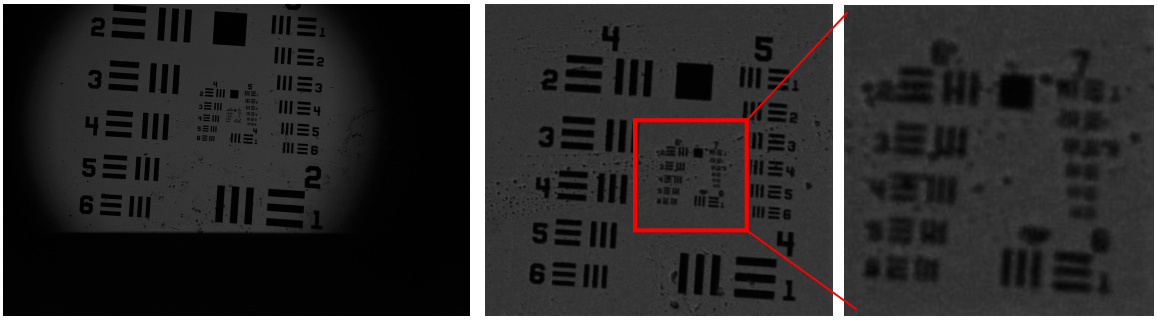

Figure 16: Image of a USAF target taken with a 5X objective and f = 200 mm Nikkor lens with a 560-nm pulsed LIF backlight. Vignetting and cropping in the full frame photo (left) are caused by focusing of the illumination beam and the camera shutter, respectively. Images at center and right are cropped from full frame (left) and scaled for visibility.

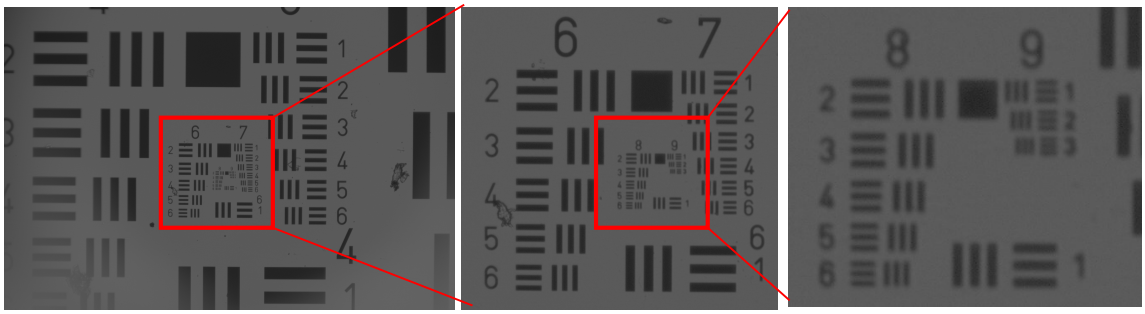

Figure 17: Image of USAF test chart taken with a 10X objective and Infinity K2S 700-mm lens with a a 450-nm pulsed-LIF backlight. Images at center and right are cropped from full frame (left) and scaled for visibility.

Figure 18 demonstrates the measured MTF for the Phase 2a and Phase 2b Spectral Microscopy systems, compared to a mirror-based long-range microscopic lens (Questar QM-1) used by Zaheer [12]. The QM-1 (**Figure 18a**) does not display the longitudinal chromatic aberration issues experienced with the glass K2 Distamax lens used in Phase 1. However, the 10% MTF resolution is around 75 lpmm, which is equivalent to 7 μm. This falls short of our diagnostic target of < 2 μm, and was therefore not considered for continued use in this project. The Phase 2a system (**Figure 18b**) has a measured 10% MTF resolution of approximately 130 lpmm, or 3.8 μm, while the Phase 2b system (**Figure 18c**) has a measured 10% MTF resolution of approximately 500 lpmm, or 1.0 μm.

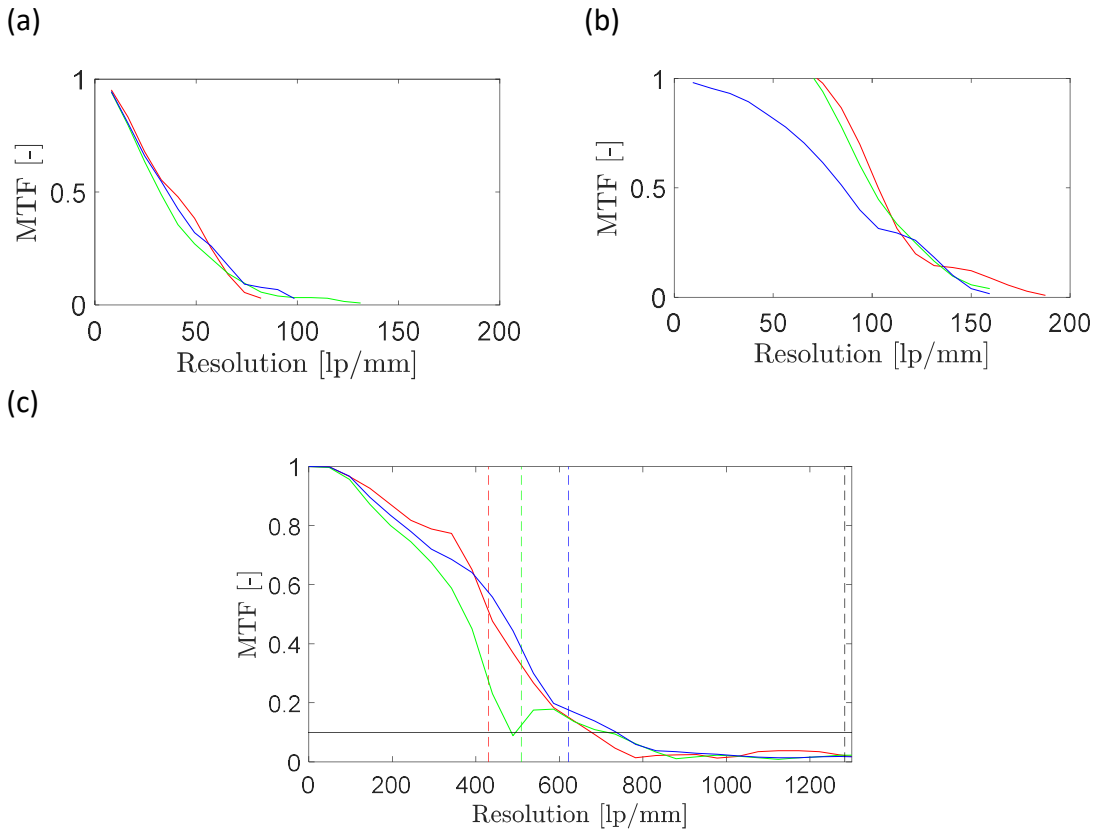

Figure 18: Measured MTF of the Phase 2a and Phase 2b Spectral Micrsocopy systems, compared to a commercial mirror-based long-range microscope (Questar QM-1). (a) Questar QM-1, (b) 5x+200-mm custom lens, and (c) 10X+700-mm custom lens.

4.3 Imaging of Primary Atomization in Real Diesel Sprays

4.3.1 Full-frame spray images

The full-frame resolution (6000 x 4000 pixels) and high repetition rate (10-20 Million fps) of the developed Spectral Microscopy system can visualize spray phenomena previously impossible to see in real-size diesel sprays. Sample full-frame images of ECN Spray D are shown in **Figure 19** and **Figure 20**, respectively, to demonstrate the extensive field-of-view and resolving power of the Spectral Microscopy imaging system. **Figure 19** demonstrates an image using the Phase 2a design, which resolves atomization from the nozzle exit to approximately 40 nozzle diameters downstream, while **Figure 20** is a representative image from the Phase 2b design, which resolves the spray for approximately 6 nozzle diameters downstream. **Figure 19** captures an extensive history of the atomization process, including the nearly smooth near-nozzle liquid jet and a more evolved state of atomization downstream, showing a diffuse cloud of droplets surrounding the spray. The change in magnification between the two system designs changes the field of view, and the change in lens design also changes the resolving power. **Figure 20** shows that the emerging liquid jet isn't nearly as smooth as it appears at lower resolution (**Figure 19**). A ripple structure on the jet surface evolves into ligament formation within one nozzle-diameter downstream and the ligament field becomes increasingly complex moving downstream, with increasing droplet production. Though the image produced by the Phase 2b system design has

higher resolving power (~1 μm), blur from out-of-focus objects is more visible in **Figure 20** is due to the narrower depth-of-field that comes with a higher NA (and higher magnification) objective.

Figure 19: Sample full-frame (6000 px height, cropped width) image from Phase 2a Spectral Microscopy design. ECN Spray D, nozzle diameter of 180 μm *μm*, 500-bar fuel pressure, 6-bar ambient pressure, 1 ms after start-of-injection.

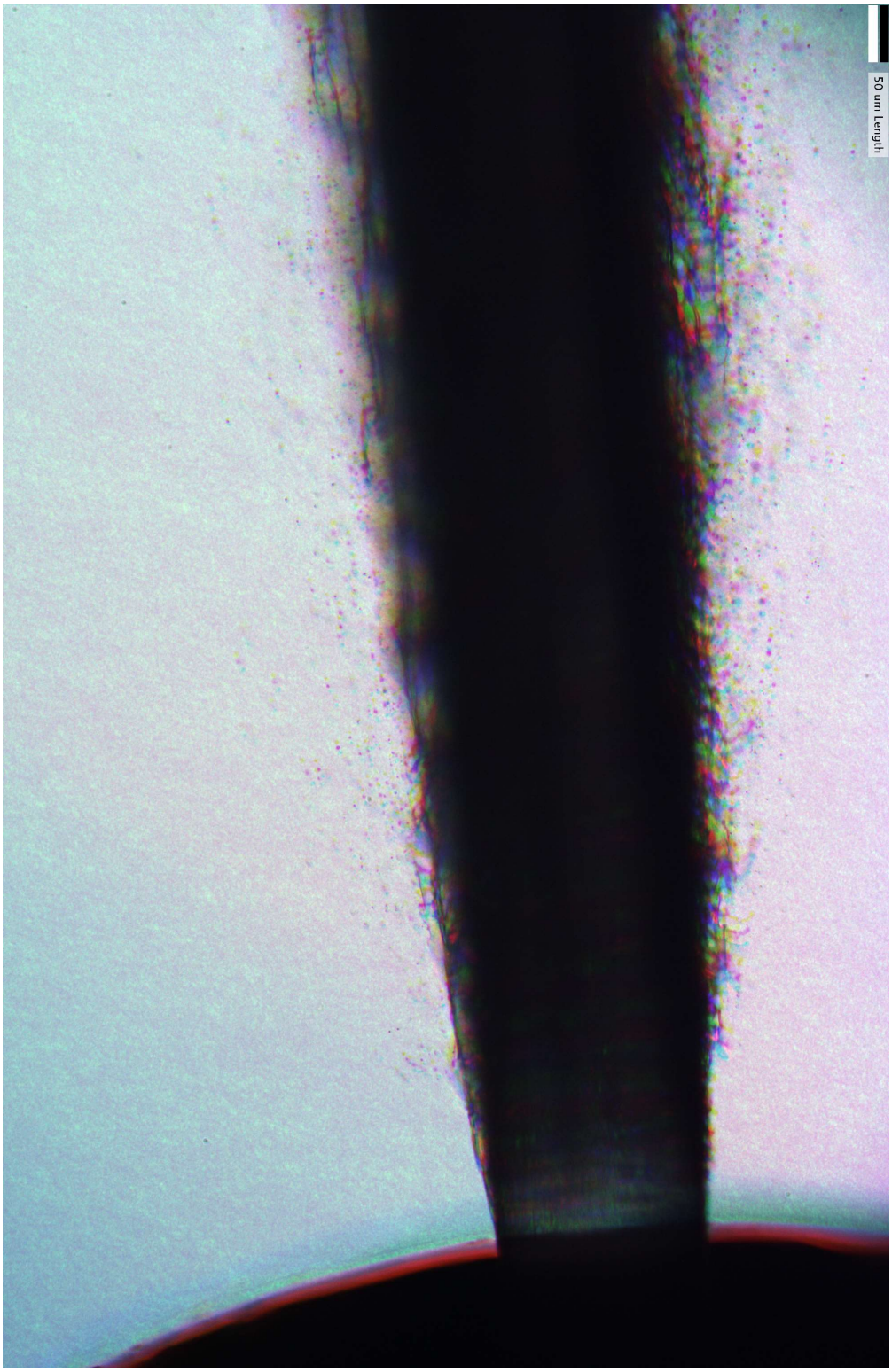

Figure 20: Sample full frame (6000 px height, cropped width) image from Phase 2b Spectral Microscopy design. ECN Spray D, nozzle diameter of 180 μm, 500-bar fuel pressure, 1-bar ambient pressure, 1 ms after start-of-injection.

4.3.2 Initial spray formation

The initial period of injection has been imaged in real diesel sprays by others [13,29]; the low-velocity flow during this period is much easier to resolve with commercial imaging systems. Images of this initial injection period from the Phase 2a system are shown in **Figure 21** (6-bar ambient pressure) and **Figure 22** (2-bar ambient pressure). A total of 120 images of initial spray formation were taken with the Phase 2b system, with 30 images distributed between four fuel pressures. Several specific features noted by others are replicated here, such as the spheroidal cap at the jet head [13,29], a leading high-velocity liquid jet/ligament preceding the head [13], droplet formation/shedding behind the jet head [30], and initial surface instabilities at the initial jet surface [29]. **Figure 21** and **Figure 22** show a more chaotic breakup structure compared to images by others, and this is likely due to the use of dodecane in our experiments, which has a lower kinematic viscosity than diesel fuel [18].

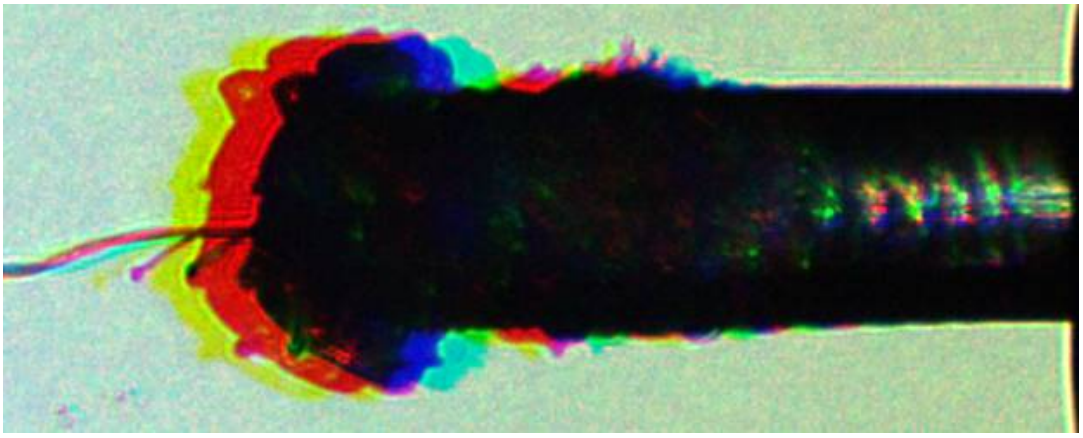

Figure 21: Initial spray formation imaged by Phase 2a system. Conditions are 500-bar fuel injection pressure and 6-bar ambient pressure. Image taken at 470 μs after start-of-injection. Nozzle diameter is 180 μm.

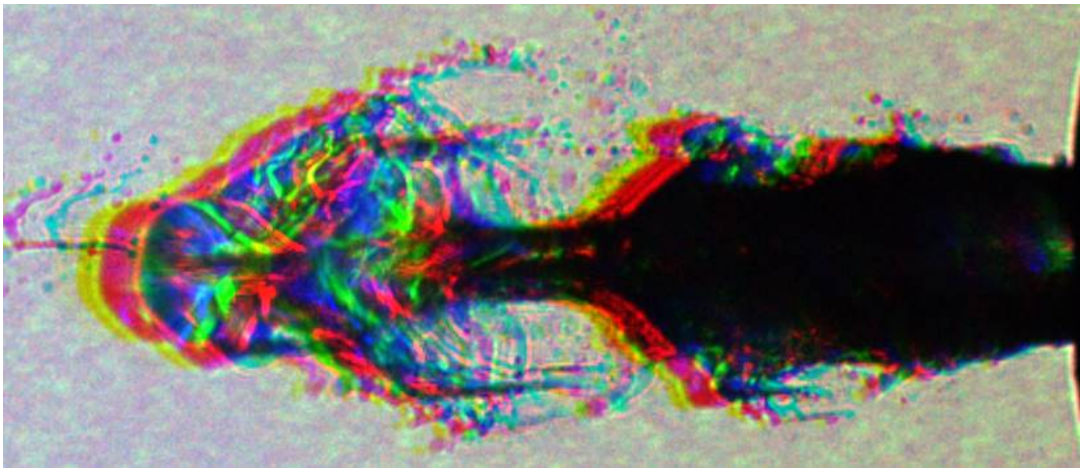

Figure 22: Initial spray formation imaged by Phase 2a system. Conditions are 500-bar fuel injection pressure and 2-bar ambient pressure. Image taken at 470 μs after start-of-injection. Nozzle diameter is 180 μm.

The images shown in **Figure 23** – **Figure 25** demonstrate the typical range of features seen during this initial injection period using the Phase 2b system design. The Phase 2b Spectral Microscopy images demonstrate improved resolution of breakup features and higher contrast due to improved light throughput. Due to facility limitations at the time of the data campaign,

ambient conditions were limited to 1-bar in this data set. **Figure 23** and **Figure 24** illustrate a common structure that occurred at the start-of-injection. In these images, a leading high-velocity jet outpaces the overall jet head, similar to that seen in [13], but the extended field-of-view of our images enables us to track these structures for a longer distance away from the nozzle exit than previously accomplished. Eventually, we see that this structure forms a smaller spheroidal cap and jet-head structure ahead of the main jet, and that the main jet head ultimately catches up to and engulfs this structure. Early droplet formation is also seen from ligaments extending from the underside of the jet head. Finally, **Figure 25** demonstrates the near-nozzle region of the liquid jet during the early-injection period, once the jet head has passed further downstream (250 μs after start-of-injection). The emerging jet has not yet achieved full velocity and the near-nozzle jet surface appears relatively undisturbed, with distinct surface waves developing some distance downstream. At this condition, the first ligament/breakup structures do not appear to form until about 3 nozzle-diameters downstream of the orifice.

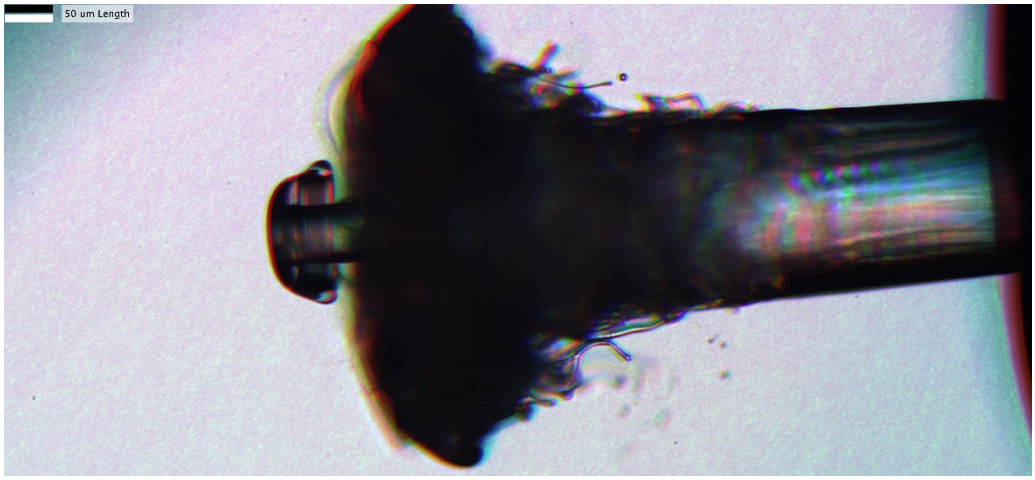

Figure 23: Initial spray formation imaged by Phase 2b system. Conditions are 500-bar fuel injection pressure and 1-bar ambient pressure. Image taken at 210 μs after start-of-injection. Nozzle diameter is 180 μm.

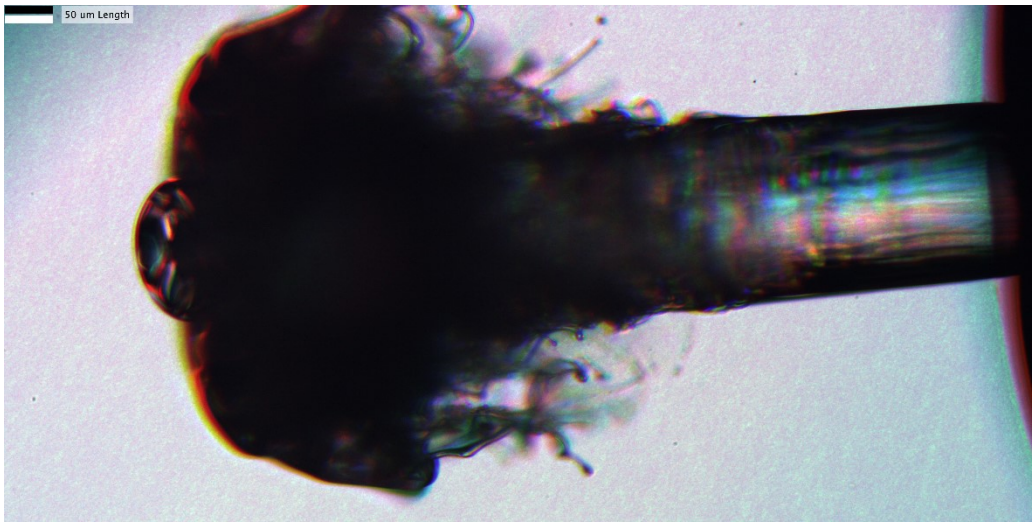

Figure 24: Initial spray formation imaged by Phase 2b system. Conditions are 500-bar fuel injection pressure and 1-bar ambient pressure. Image taken at 210 μs after start-of-injection. Nozzle diameter is 180 μm.

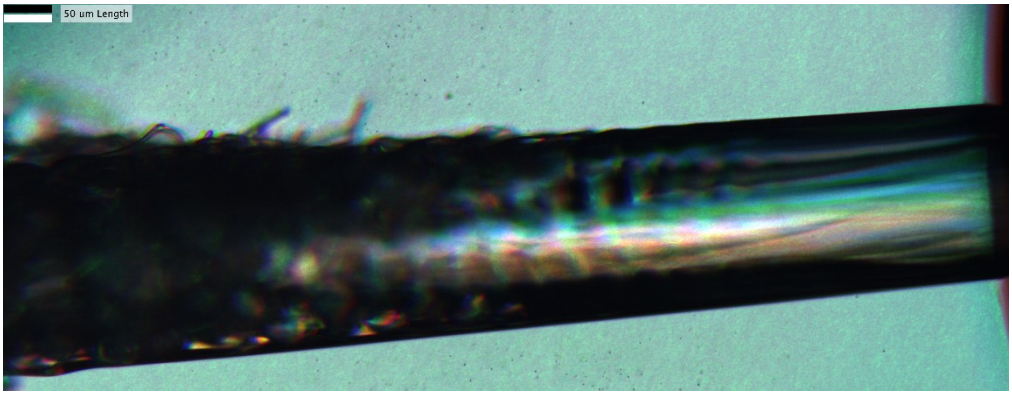

Figure 25: Initial spray formation imaged by Phase 2b system. Conditions are 350-bar fuel injection pressure and 1-bar ambient pressure. Image taken at 250 μs after start-of-injection. Nozzle diameter is 180 μm.

4.3.3 Imaging of intact core at steady-state injection

Prior researchers have proposed that, even though primary breakup in the atomization regime should begin promptly at the nozzle exit, there is an intact liquid core extending downstream until primary atomization is complete [31,32]. However, measurements to date have not proven a consensus on this [3]. Our highly-resolved images of primary atomization in real diesel sprays demonstrate evidence for this intact liquid core. This is evident by the bright regions seen extending from the nozzle exit, where light is transmitted through the liquid core uninterrupted by disturbances in the interfacial structure [33,34] With the Phase 2 high-resolution Spectral Microscopy design, the intact liquid structure is well visualized at these conditions (**Figure 25** and **Figure 26**).

Though more visible at low fuel injection pressure and during the relatively undisturbed initial fuel-injection period (**Figure 25**), an intact liquid core was also imaged at higher injection-pressures and during steady-state injection. An image of the intact core at 350-bar fuel injection pressure at full flow rate (steady-state injection) is shown in **Figure 26**. As fuel injection pressure increases, the light passing through the intact core eventually diminishes. This is shown in **Figure 27** for a fuel-injection pressure of 1500 bar. One hypothesis consistent with others is that the higher fuel pressures causes atomization to begin closer to the nozzle exit [35], so that light does not pass through the core without scattering.

To better visualize the intact liquid core, we modified the illumination setup, placing a diffuser within the spray chamber, just behind the spray. Preliminary images using the near-field diffuser illuminate the intact liquid core brighter than images without the near-field diffuser. A diffuser increases the ratio of diffuse/direct light rays, thus reducing the effect of light extinction due to scattering. A sample image is shown in **Figure 28**. The image is not perfectly focused, as it was taken with a prototype lens setup that was not well aligned. However, illumination is seen passing through the core of the jet for several nozzle-diameters downstream (across the entire field-of-view of this image). This suggests that accurate measurement of the liquid core is dependent on the illumination characteristics of the system. Further, it also implies that intact liquid regions exist in real diesel sprays and that they extend further downstream than previously anticipated [33].

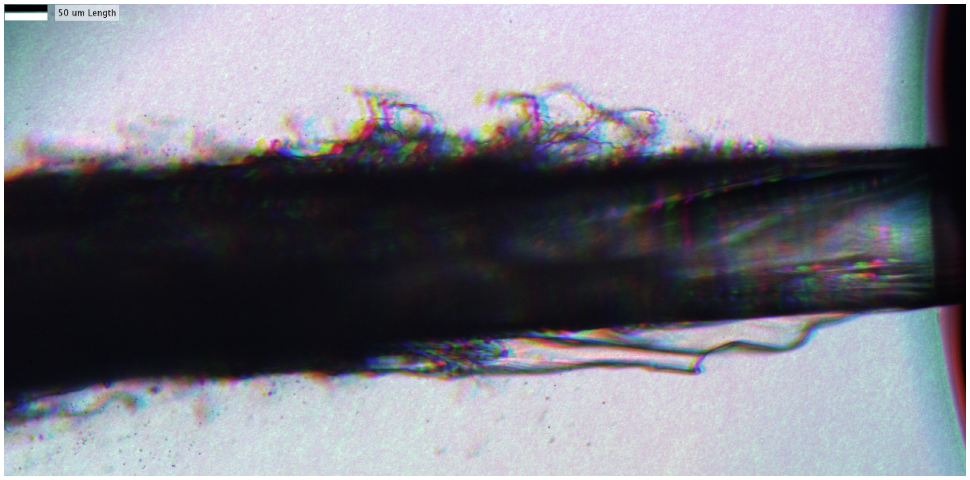

Figure 26: Steady-state injection imaged by Phase 2b system. Conditions are 300-bar fuel injection pressure and 1-bar ambient pressure. Image taken at 1 ms after start-of-injection. Nozzle diameter is 180 μm.

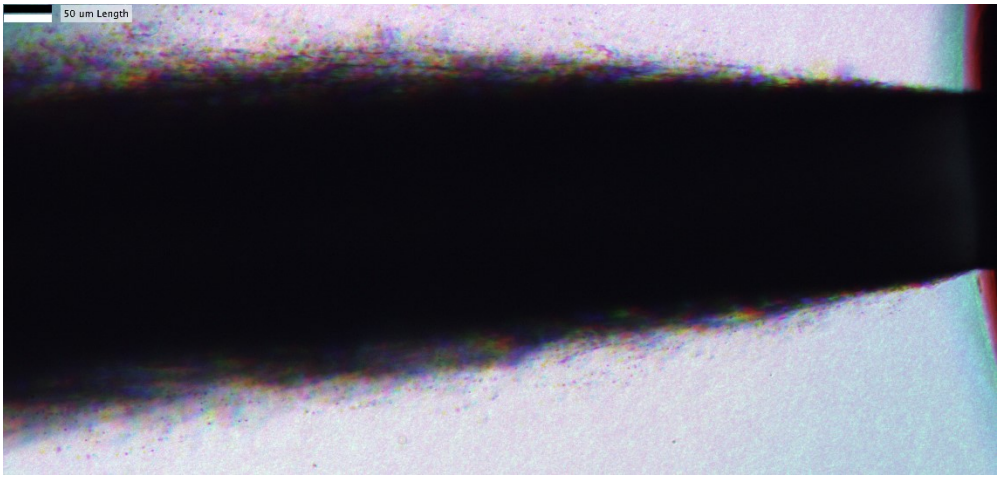

Figure 27: Steady-state injection imaged by Phase 2b system. Conditions are 1500-bar fuel injection pressure and 1-bar ambient pressure. Image taken at 1 ms after start-of-injection. Nozzle diameter is 180 μm.

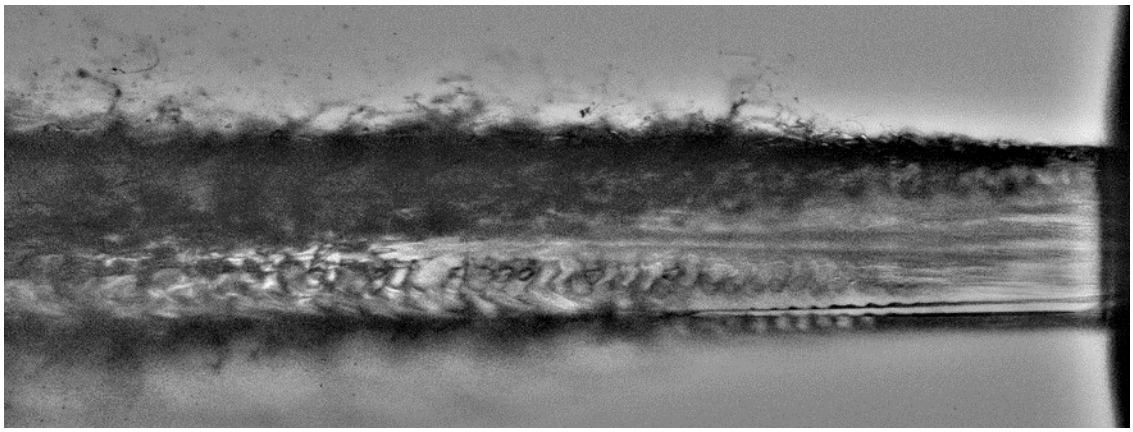

Figure 28: Monochromatic image of steady-state injection at 400-bar fuel injection pressure injecting into 1-bar ambient pressure. Image taken at 1 ms into a 2 ms injection event.

4.3.4 Visualization and quantification of surface instabilities

The Spectral Microscopy system is also able to resolve surface wave instabilities forming on the near-nozzle liquid surface during steady-state injection conditions. The prevailing primary atomization theory used for diesel spray modeling in CFD codes assumes that primary atomization arises from surface Kelvin-Helmholtz instabilities that grow to form droplets with diameters on the scale of the fastest growing wavelength [4]. This theory suggests that these waves are sub-micron in scale for diesel injection conditions, and thus they have not been resolved in prior imaging experiments at steady-state (high velocity) flow conditions.

Figure 29 shows an example of these instabilities, as captured by the Phase 2b imaging system, imaged at steady-state injection conditions for the first time. Here, the red, green, and blue banding show the wave structure moving in time. The wavelengths measured from these images are on the order of 10 μm, rather than the order of 1 μm predicted by Reitz [4].

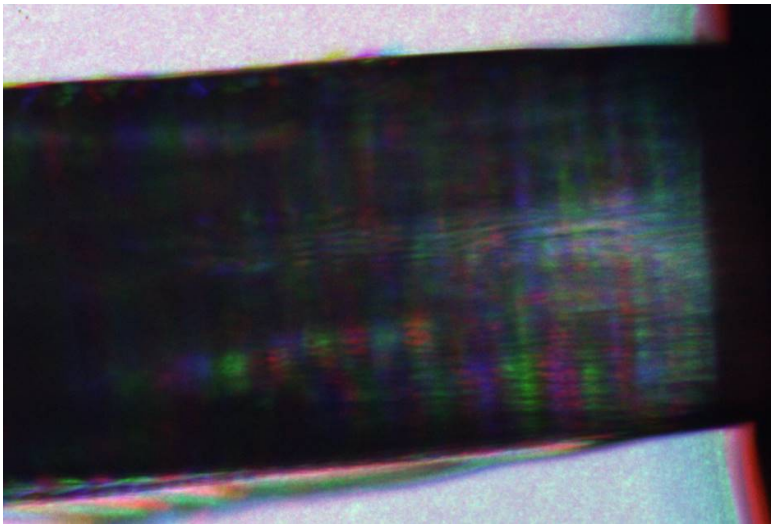

Figure 29: Surface waves imaged by Phase 2b system near nozzle during steady-state fuel injection. Conditions are 300-bar fuel injection pressure and 1-bar ambient pressure. Image taken at 1 ms after start-of-injection. Nozzle diameter is 180 μm.

Images from Phase 2a were analyzed to quantify the near-nozzle surface wavelengths at varying ambient backpressures. The average visible surface wavelength for each condition is compared to the Kelvin-Helmholtz model-predicted wavelength for the fast growing (most ustable) surface wave [4], as shown in **Figure 30**. A linear relationship is measured between the predicted fastest-growing wavelength and the measured surface wavelength from Spectral Microscopy imaging. The correlation strength at 2-bar ambient pressure is the weakest, which may be expected since lower ambient pressures reduce the aerodynamic forces responsible for Kelvin-Helmoholtz breakup. However, the measured wavelengths (O ~ 10-20 μm) are an order of magnitude larger than those predicted by the Kelvin-Helmholtz model (O ~ 1 μm). Thus, the instabilities visualized are not likely Kelvin-Helmholtz surface instabilities, but are more likely instabilities stemming from a different fluid phenomena.

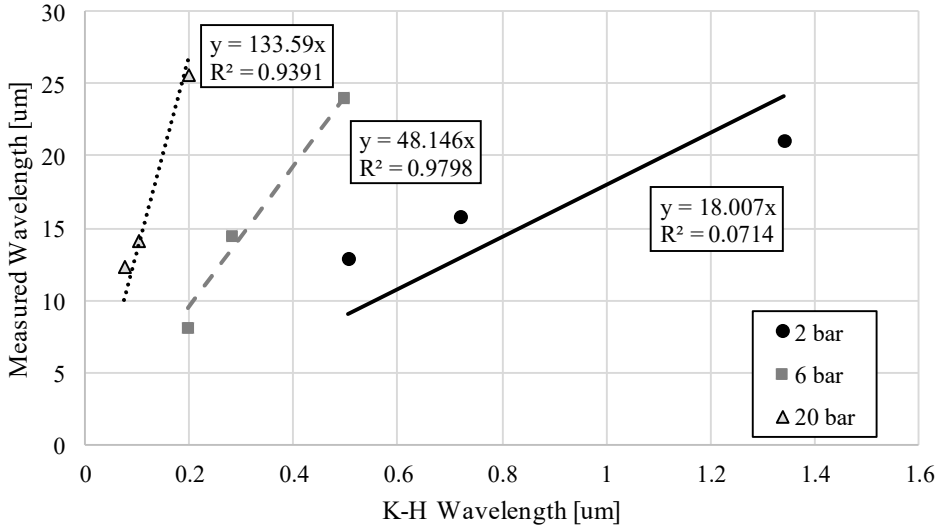

Figure 30: Kelvin-Helmholtz model most unstable wavelength relative to measured surface wavelength from Phase 2a images of steady state injections.

4.3.5 Ligament and droplet formation

Using the system design with the highest resolution capabilities (Phase 2b), the Spectral Microscopy system was used to image ligament and droplet formation in ECN Spray D. Over 250 images were obtained for sprays during steady-state injection, injected into a 1-bar ambient pressure, using fuel injection pressures of 300, 500, 1000 and 1500 bar. In this study, we aimed to establish the operating condition limits for resolved primary breakup imaging of Spray D.

A set of sample images for a low fuel injection pressure (300 bar) is shown in **Figure 31**. The images have a 2 μm square at the top left to indicate scale and the image sequences from left to right are taken 75 ns apart. Most images show drop formation stemming from the breakup of very long, narrow ligament structures. This is exemplified in **Figure 31(c)** and **(e)**. The scale of atomization is also another point of interest. In **Figure 31(a)**, **(d)**, and **(e)**, most droplets are on the scale of 2-10 microns, while the ligaments that form them are similar diameter but on the order of 10-50 μm long. Notably, the scale of ligament and droplet formation does not appear to well correlate with the scale of observed surface waves near the nozzle, which are an order of magnitude larger. The primary atomization process appears driven by other instability sources that are much smaller in scale.

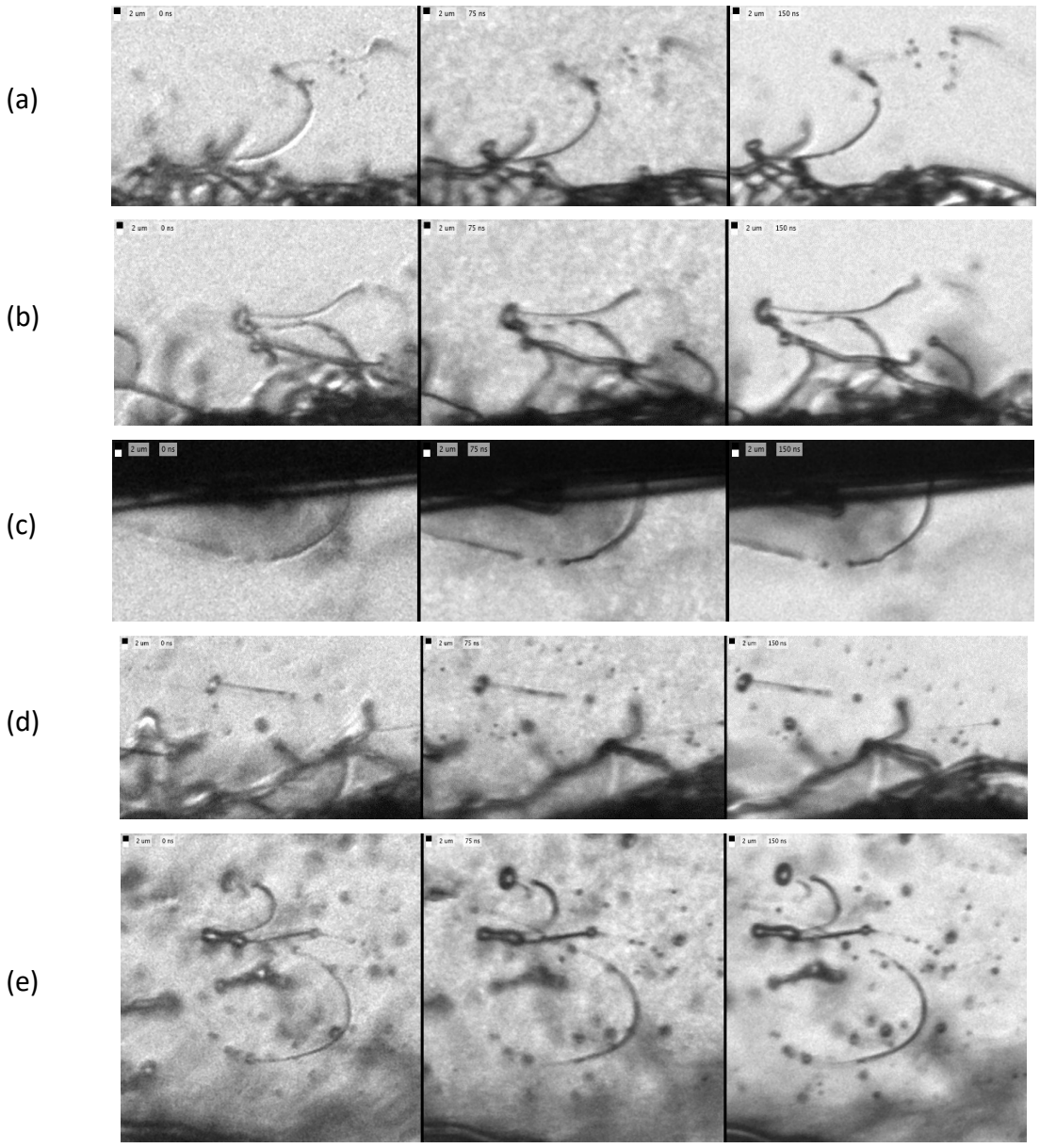

Figure 31: Ligament and droplet formation at the periphery Spray D at 300-bar fuel injection pressure, steady-state injection conditions. Small square shown at top-left of images is 2 μm in scale.

Figure 32 shows images of ligament and droplet formation at higher fuel injection pressures. In the first two rows**, Figure 32(a)** and **(b)** show the typical ligament droplet field for a fuel injection pressure of 500 bar. The fields are generally more chaotic and the scale of the structures is reduced. As seen at lower injection pressure (**Figure 31**), droplets are generally formed from the stretching/pinching and breakup of long ligament structures. Measureable droplets that are in focus are typically on the order of 1-2 μm. **Figure 32(c)** and **(d)** show the typical ligament droplet field for a fuel injection pressure of 1000 bar. The ligaments stuctures become even longer at this condition, now on the order of 100 μm in length. These ligaments appear to be the main source for droplet production, at least at the periphery of the spray were imaging can be executed. The ligaments stretch/pinch and breakup into droplets near 1 μm in

scale. Droplet formation at this condition is at the edge of the system resolution and as a result, the smallest structures appear more defocused, regardless of their position with respect to the focus plane. Finally, **Figure 32(d)** shows the typical ligament droplet field for a fuel injection pressure of 1500 bar. As fuel injection pressure increases above 1000 bar, the scale of atomization decreases and structures in the image become difficult to resolve. The ligament and droplet structures in **Figure 32(d)** appear blurred because they are smaller than the resolving power of the system. This indicates that these structures are sub-micron in scale and that droplets produced by diesel sprays at real injection pressure (> 1000 bar) are sub-micron, at least at the spray periphery.

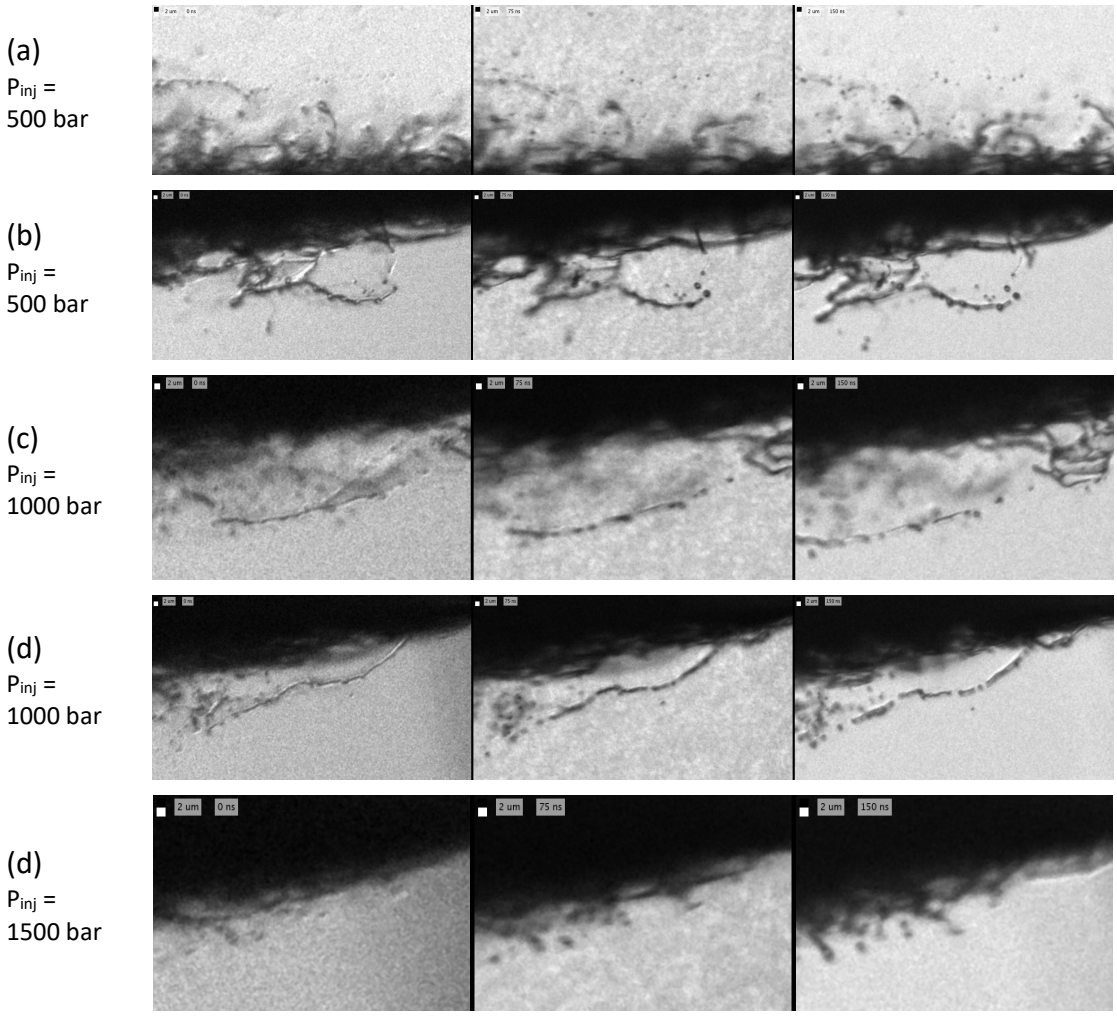

Figure 32: Ligament and droplet formation at the periphery Spray D at fuel injection pressures of 500 bar (a) and (b), 1000 bar (c) and (d), and 1500 bar (e). Steady-state injection conditions. Small square shown at top-left of images is 2 μm in scale.

5 Summary of Conclusions

4.1 Spectral Microscopy Imaging with High-Power Pulsed-LED Illumination

- High-power pulsed LEDs did not provide sufficient illumination output for ns-scale, μm-scale microscopy. Even with optimized optical train design, poor light throughput resulted in degraded image contrast and resolution (limited to approximately 3 μm), well below the diffraction-limited performance of the microscopic lens (1.9 μm).
- Though the long-range microscopic lens initially implemented (Infinity K2 Distamax) had excellent specified resolution performance (down to 1.9 μm), it suffered from significant longitudinal chromatic aberration (~1 mm variation in focus plan between red/green and blue light). This aberration degraded resolution of the Spectral Microscopy system even further, limiting the maximum resolution of the system to approximately 33 μm, well below the target resolution of < 2 μm.

4.2 Novel Two-Piece Microscopy Lens Design

- A custom two-piece lens design enabled imaging at shorter working distances, significantly increasing magnification (up to 0.2 μm/px, 19.5x magnification) and resolution (down to 1 μm). The two-piece design also enabled high-resolution imaging of sprays injected in to a high-pressure environment because the objective is physically decoupled from the main body lens and can be mounted inside the spray chamber.
- A novel three-color pulsed-LIF illumination system produced sufficient light throughput to realize theoretical diffraction-limited resolution performance (down to 1 μm) and was demonstrated at imaging speeds of up to 13 Mfps.

4.3 Imaging of Primary Atomization in Real Diesel Sprays

4.3.1 Full-frame spray images

- The high-resolution 24-MP camera sensor used in this work enabled a substantial history of the atomization process to be captured without sacrificing spatial or temporal resolution. We demonstrate full-frame imaging of ECN Spray D using two custom lens setups. Using the Phase 2a setup, we demonstrate a field-of-view from the nozzle exit to ~40 nozzle diameters downstream at 3.8 μm resolution and at a framing rate of 3 Mfps. Using the Phase 2b setup, we demonstrate a field-of-view from the nozzle exit to ~6 nozzle diameters downstream at 1 μm resolution and at a framing rate of 13 Mfps

4.3.2 Initial spray formation

- Imaging of the liquid jet emerging from the fuel injector during start-of-injection demonstrated several breakup features noted previously by others, including the spheroidal cap at the jet head [13,29], a leading high-velocity liquid jet/ligament preceding the head [13], droplet formation/shedding behind the jet head [30], and initial surface instabilities at the initial jet surface [29].

4.3.3 Imaging of intact core at steady-state injection

- Prior measurements in the literature do not reach consensus on the presence of an intact liquid core in real diesel sprays [3], but we see evidence for an intact liquid core extending from the nozzle exit of ECN Spray D in nearly all images taken throughout the project. The intact core is most clearly imaged at low fuel-injection pressure and at the start of injection, but it is also seen at higher injection pressure and during steady-state fuel injection. The visibility of an intact liquid core decreases with increasing fuel injection pressure, consistent with observations and predictions by others [32,31,35].
- The extent of the observed liquid core, as evidenced by the passage of undisturbed light through the jet, is dependent on the optical setup. When we placed a near-field diffuser directly behind the spray, direct light transmission was seen in regions of the spray core extending several nozzle-diameters downstream (across the entire field-of-view).

4.3.4 Visualization and quantification of surface instabilities

- Surface waves were imaged at the liquid interface of the emerging liquid jet from a real diesel injector (ECN Spray D) under steady-state injection conditions. This phenomenon has not been previously resolved for real diesel sprays.
- The measured surface wavelengths (O ~ 10-20 μm) are an order of magnitude larger than those predicted by the Kelvin-Helmholtz model (O ~ 1 μm) used widely for CFD simulation of diesel spray combustion. Thus, the instabilities visualized are not likely Kelvin-Helmholtz surface instabilities, but more likely stem from a different fluid phenomenon.

4.3.5 Ligament and droplet

- Ligament and droplet formation was imaged for a real diesel injector (ECN Spray D) under steady-state injection conditions. These phenomena have not been previously resolved at steady-state conditions in real diesel sprays.
- Most images show drop formation stemming from the breakup of very long, narrow ligament structures. At low injection pressures (300 bar), most droplets are on the scale of 2-10 μm, while the ligaments that form them are similar diameter but on the order of 10-50 μm long. At higher injection pressures (1000 bar), the ligaments increase in length to around 100 μm, with diameters near 1 μm. The ligaments were commonly observed to experience a Rayleigh-type breakup, where surface tension forces appeared to drive breakup of the thin ligaments into strands of droplets on the scale of the ligament diameter.
- Ligaments and droplets could not be perfectly resolved by the Spectral Microscopy system at a fuel injection pressure of 1500 bar. This implies that the ligament and droplet diameters are sub-micron in scale, below the 1-μm resolving power of the imaging system.
- The scale of ligament and droplet formation does not appear to well correlate with the scale of observed surface waves near the nozzle, which are an order of magnitude larger. The primary atomization process appears driven by other instability sources that are much smaller in scale.

References

1. Sallam, K.A. and Faeth G.M. (2003). Surface Properties During Primary Breakup of Turbulent Liquid Jets in Still Air. *AIAA Journal*, 41(8):1514-1524.

2. Sallam, K.A., Dai, Z., and Faeth, G.M. (2002). Liquid Breakup at the Surface of Turbulent Round Liquid Jets in Still Gases. *Int. J. of Multiphase Flow*, 28:427-449.

3. Dumouchel, C. (2008). On the Experimental Investigation on Primary Atomization of Liquid Streams. *Exp. Fluids*, 45:371-422

4. Reitz, R.D. and Bracco, F.V. (1982). Mechanism of Atomization of a Liquid Jet. *Phys. Fluids*, 25(10):1730-1742.

5. Reitz, R.D. and Bracco, F.V. (1979). On the Dependence of Spray Angle and Other Spray Parameters on Nozzle Design and Operating Conditions. *SAE Technical Paper* 790494.

6. Reitz, R.D. and Bracco, F.V. (1979). Ultra-High-Speed Filming of Atomizing Jets. *Phys. Fluids*, 22(6):1054-1064.

7. Beale, J. C., & Reitz, R. D. (1999). Modeling spray atomization with the Kelvin-Helmholtz/Rayleigh-Taylor hybrid model. *Atomization and Sprays*, 9(6), 623-650.

8. Som, S., & Aggarwal, S. K. (2010). Effects of primary breakup modeling on spray and combustion characteristics of compression ignition engines. *Combustion and Flame*, *157*(6), 1179-1193.

9. Som, S., Longman, D. E., Ramírez, A. I., & Aggarwal, S. K. (2010). A comparison of injector flow and spray characteristics of biodiesel with petrodiesel. *Fuel*, *89*(12), 4014-4024.

10. Kirsch, V., Reddemann, M.A., Palmer, J., and Kneer, R. (2017). Zooming into primary breakup mechanisms of high-pressure automotive sprays. *Proceedings of ILASS–Europe*, September 6-8, 2017.

11. Desjardins, O. and Pitsch H. (2010). Detailed Numerical Investigation of Turbulent Atomization of Liquid Jets. *Atom. Sprays*, 20(4):311-336.

12. Zaheer, H. and Genzale, C.L. (2015). Transient Microscopy of Primary Atomization in Gasoline Direct Injection Sprays. *Proceedings of ILASS-Americas*, May 2015.

13. Crua, C., Heikal, M.R., and Gold, M.R. (2015). Microscopic imaging of the initial stage of diesel spray formation," *Fuel*, 157, 140–150.

14. Linne, M.A., Paciaroni, M., Berrocal, E., and Sedarsky, D. (2009). Ballistic imaging of liquid breakup processes in dense sprays. Proceedings of the Combustion Institute, 32, 2147-2161.

15. Lai, M.-C., Zheng, Y., Xie, X.-B., Moon, S., Liu, Z., Gao, J., Zhang, X., Fezzaa, K., Wang, J., and Shi, J. (2011). Characterization of the Near-Field Spray and Internal

Flow of Single-Hole and Multi-Hole Sac Nozzles using Phase Contrast X-Ray Imaging and CFD. *SAE International Journal of Engines*, 4(1):703-719.

16. Kastengren, A. *et al.*(2017). Measurements of droplet size in shear-driven atomization using ultra-small angle x-ray scattering. *Int. J. Multiph. Flow*, 92, 131–139.
17. Feng, Z., Tang, C., Yin, Y., Zhang, P. and Huang, Z. (2019). Time-resolved droplet size and velocity distributions in a dilute region of a high-pressure pulsed diesel spray. *Int. J. Heat Mass Transf.*, 133, 745–755.
18. International Organization for Standardization. (2017). Photography - Electronic Still Picture Imaging - Resolution And Spatial Frequency Responses. ISO 12233:2017.
19. Clemens, N.T. (2002). Flow Imaging. *Encycl. Imaging Sci. Technol.*, 390–419.
20. Aguirre-Pablo, A.A., Alarfaj, M.K., Li, E.Q., Hernández-Sánchez, J.F., and Thoroddsen, S.T. (2017). Tomographic Particle Image Velocimetry using Smartphones and Colored Shadows. *Sci. Rep.*, vol. 7, no. 1, pp. 1–18.
21. Funatani, S., Takeda, T., and Toriyama, K. (2014). High-Resolution Three-Color Piv Technique Using a Digital Slr Camera. *J. Flow Vis. Image Process.*, vol. 20, no. 1–2, pp. 35–45.
22. McGregor, T.J., Spence, D.J. and Coutts, D.W. (2008). Laser-based volumetric flow visualization by digital color imaging of a spectrally coded volume. *Rev. Sci. Instrum.*, vol. 79, no. 1.
23. Sigernes, F., Dyrland, M., Peters, N., Lorentzen, D.A., Svenøe, T., Heia, K., Chernouss, S., Deehr, C.S. and Kosch, M. (2009). The absolute sensitivity of digital colour cameras. *Optics Express,* 17(22).
24. Menser, J., Dreier, T., Kaiser, S., and Schulz, C. (2015). Multi-pulse RGB illumination and detection for particle tracking velocimetry. *Proceedings of the 7th European Combustion Meeting,* 1–6.
25. Jaw, S.-Y., Sheen, J.-J., and Hwang, R. (2014). Development and Application of an Alternating-Color Micro-PIV System. *Proceedings of the ASME 2014 International Mechanical Engineering Congress and Exposition*, 1–8.
26. Knox, B. and Genzale, C. (2016). Effects of End-of-Injection Transients on Combustion Recession in Diesel Sprays. *SAE Int. J. Engines*, 9(2), 932–949.
27. Sandia National Labs, "Engine Combustion Network | Spray D Nozzle Geometry," 2018. [Online]. Available: https://ecn.sandia.gov/diesel-spray-combustion/target-condition/spray-d-nozzle-geometry/. [Accessed: 16-Apr-2019].
28. Reitz, R.D. (1978). Atomization and other Breakup Reigmes of a Liquid Jet. Ph.D. Thesis, Princeton University, Princeton, NJ.
29. Kirsch, V. *et al.* (2019). Transparent high-pressure nozzles for visualization of nozzle internal and external flow phenomena," *Rev. Sci. Instrum.*, 90(3).
30. Shinjo, J. and Umemura, A. (2010). Simulation of liquid jet primary breakup: Dynamics of ligament and droplet formation. *Int. J. Multiph. Flow*, 36(7), 513–532.

31. Reitz, R. D. and Diwakar, R. (1987). Structure of high-pressure fuel sprays. *SAE transactions*, 96(5), 492-509.

32. Chehroudi, B., Chen, S.H., Bracco, F.V., and Onuma, Y. (1985). On the intact core of full-cone sprays. *SAE Tech. Paper No. 1985-02-01*.

33. Pickett, L.M., Manin, J., Kastengren, A. and Powell, C. (2014). Comparison of Near-Field Structure and Growth of a Diesel Spray Using Light-Based Optical Microscopy and X-Ray Radiography. *SAE Int. J. Engines*, 7(2), 1044–1053.

34. Yon, J., Blaisot, J.-B., and Ledoux, M. (2014). Unusual Laser-Sheet Tomography Coupled With Backlight Imaging Configurations To Study the Diesel Jet Structure At the Nozzle Outlet for High Injection Pressures. *J. Flow Vis. Image Process.*, 9(1),19.

35. Arai, M., Shimizu, M., Hiroyasu, H. (1988). Break-up length and spray formation mechanism of high speed liquid jet. *Proceedings of ICLASS 1988*, Sendai, Japan, 177–184.